Circulation in Drake Passage revisited using new current time series and satellite altimetry: 1. The Yaghan Basin

Ramiro Ferrari, Christine Provost, Alice Renault, Nathalie Sennéchael, Nicolas Barré, Young-Hyang Park, Jae Hak Lee

Circulation in Drake Passage revisited using new current time series and satellite altimetry: 1. The Yaghan Basin

Ramiro Ferrari,[1] Christine Provost,[1] Alice Renault,[1] Nathalie Sennéchael,[1] Nicolas Barré,[1] Young-Hyang Park,[1] and Jae Hak Lee[2]

[1]   The complex bathymetry of the Drake Passage and the meridional extent of the Shackleton Fracture Zone, in particular, force the Subantarctic Front (SAF) and the Polar Front (PF) to veer to the north, and the flow of the Antarctic Circumpolar Current concentrates in the Yaghan Basin. We have studied the circulation in the Yaghan Basin, using 3 years of velocity data (January 2006–March 2009) at five mooring sites and 18 years of satellite altimetry data. Mean velocities at our mooring sites show a dominant eastward component which decreases with depth, as expected, with a notable exception in the center of the Yaghan Basin, where mean velocities reveal a dominant westward component increasing with depth. The mooring data suggest the existence of a permanent, strong deep cyclonic circulation over the Yaghan seafloor depression in the northeastern part of the Yaghan Basin. The in situ data provide the first opportunity to compare altimetry-derived velocities with high temporal resolution near-surface current meter velocities in a large eddy kinetic energy environment at high latitudes. Globally, altimetry-derived velocities compare rather well with the in situ velocities at 500 m depth both in strength and direction. Correlations are high between the in situ velocities and the surface velocities derived from satellite altimetric data. Mean sea level estimates lead to reasonable mean surface velocities with, however, a slight underestimation of the mean velocity at the mean location of the SAF on the continental slope and a more important underestimation of the westward current in the center of the Yaghan Basin. A dominant mode of velocity variations (23% of the variance) is observed both in the in situ and satellite data, corresponding to a strong southward meander of the SAF upstream of the mooring line and a northward meander of the PF downstream of the latter. The 18 yearlong altimetry time series shows that the mode is robust and has a strong semiannual component.

1.   Introduction

[2]   The Antarctic Circumpolar Current (ACC) is the only current to circumnavigate the globe and is the largest wind-driven current in the world. This is made possible by an obstacle-free latitudinal zone in the Southern Ocean. It plays an important role in global climate by connecting all the major oceans, transporting water and properties.

[3]   The ACC consists of a number of circumpolar fronts, which correspond to water mass boundaries near the surface and to deep-reaching jets [*Nowlin et al.*, 1977; *Orsi et al.*, 1995]. Velocities are large in the jet cores (>50 cm s^{-1}) leading to large total ACC transport (e.g., about 134 ± 11 Sv [*Renault et al.*, 2011]). Topography plays an important role in controlling the ACC transport although the precise modalities (bottom torque, friction, instabilities, eddy fluxes…) are not fully resolved or understood.

[4]   Located between the South American and Antarctic continents, Drake Passage (DP) is the narrowest stretch of water separating Antarctica from other continents (by a distance of about 800 km), and exerts a strong constraint on both the path and the strength of the ACC. The Drake

[1]LOCEAN, UMR 7159, CNRS/UPMC/MNHN/IRD, Université Pierre et Marie Curie, Paris, France.
[2]Korean Ocean Research and Development Institute, Seoul, South Korea.

Corresponding author: R. Ferrari, LOCEAN, UMR 7159, CNRS/UPMC/MNHN/IRD, Université Pierre et Marie Curie, T. 45/46 5e étage, 4, place Jussieu, FR-75252 Paris CEDEX 05, France. (ramiro.ferrari@locean-ipsl.upmc.fr)
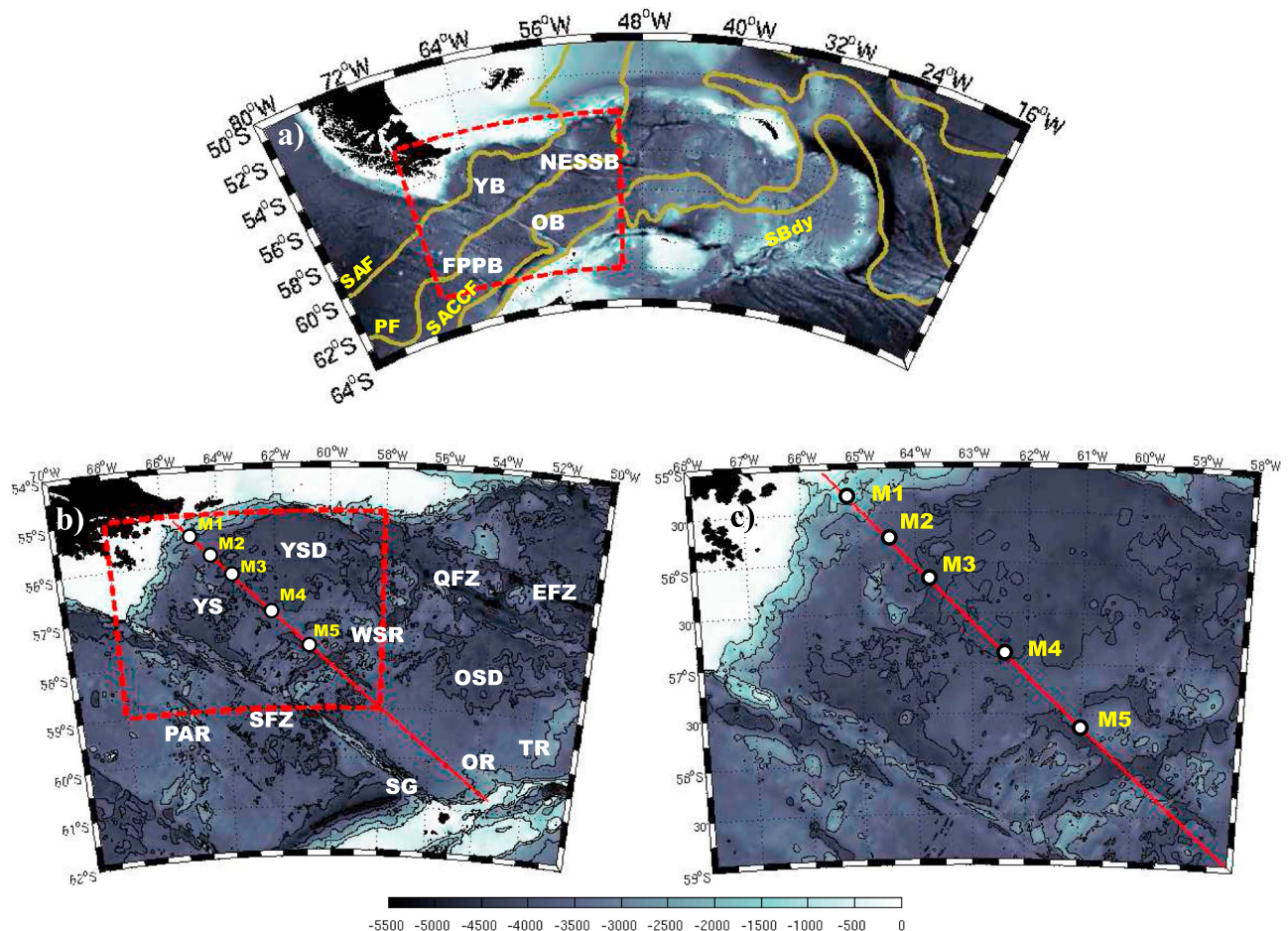
Figure 1. Bottom topography (in meters) and locations of the current meter moorings at Drake Passage. (a) Bottom topography of the Drake Passage with the main basins labeled: Yaghan Basin (YB), Ona Basin (OB), Former Phoenix Plate Basin (FPPB), and Northeast Scotia Sea Basin (NESSB). The yellow lines indicate the mean location of the major fronts, according to *Orsi et al.* [1995], from north to south: SAF, Subantarctic Front; PF, Polar Front; SACCF, South ACC Front; SBdy, southern boundary of the ACC. (b) White points indicate the locations of the moorings deployed along the Jason ground track 104 (red line) in the Yaghan Basin in January 2006. Major ridges or fracture zones are indicated: Shackleton Fracture zone (SFZ); Phoenix Antarctic Ridge (PAR); West Scotia Ridge (WSR); Ona Seafloor Depression (OSD); Ona Rise (OR) and Terror Rise (TR); Yaghan Seamounts (YS); Quest Fracture Zone (QFZ); Endurance Fracture Zone (EFZ); Yaghan Seafloor Depression (YSD); and the Shackleton Gap (SG). (c) Zoom on the mooring sites. Isobaths (1000, 2000, 3000, 4000 and 5000 m) are plotted.

Passage acts as a choke point for the ACC and logistically it is the most practical location at which to monitor the ACC; it is here that the full meridional extent of the ACC can be most easily spanned. Consequently, the DP is the region of the Southern Ocean that has been the most intensively sampled. This Passage is crisscrossed by a number of fracture zones (Figure 1a). The Shackleton Fracture Zone (SFZ), which rises to a depth of about 1500 m in the southern half of the DP, deflects the ACC fronts northward. The northern half of the DP is the site of local maxima in eddy kinetic energy, which is particularly high at the entrance to and the exit from the Yaghan Basin [*Barré et al.*, 2011]. *Sokolov and Rintoul* [2009] showed that the principal ACC fronts comprised multiple branches along the path of the ACC and that they tend to converge into the three main jets (the Subantarctic Front, the Polar Front and the Southern ACC front) as

they enter Drake Passage. Topography favors recurrence of some meanders and eddies at specific places in DP. For example, a dipole occurring with a close-to-annual periodicity is observed at the entrance to DP over the northern part of the Phoenix Antarctic Ridge (PAR) and the SFZ (Figure 1b) and corresponds to adjacent meanders of the SAF and PF [*Barré et al.*, 2011].

[5] *Meredith et al.* [2011] thoroughly reviewed the past and present monitoring in the DP and the major breakthroughs that resulted from this activity concerning the complex structure of the ACC, the quantification of the ACC transport, the Southern Ocean overturning circulation etc. Major in situ velocity measurements in DP are recalled. Apart from providing the first yearlong estimated transport time series [*Whitworth*, 1983], mooring data from the landmark DRAKE 79 field experiment provided fundamental

insights into the spatial and temporal structure of the flow. In particular, the vertical shear was observed to vary on large vertical scales [e.g., *Hofmann and Whitworth*, 1985]; current variability was characterized by red spectra with time scales of 20–50 d in general and by some higher frequencies near steep topography [e.g., *Inoue*, 1985]; topography was shown to be instrumental in frontal meander and eddy genesis [e.g., *Klinck*, 1985]. Later, lowered acoustic Doppler profilers (LADCP) from hydrographic cruises provided instantaneous high vertical resolution full depth current observations [e.g., *Cunningham et al.*, 2003; *Renault et al.*, 2011] and a repeat shipboard ADCP line (high vertical resolution in the upper 1000 m of the water column) [*Firing et al.*, 2011] confirmed that the geostrophic shear varies on large vertical scales. Near–bottom velocities in DP acquired over a wide array within the recent c-Drake experiment (2007–2011) revealed large near-bottom velocities with peak values (note that a velocity is a speed with a direction as well) of 0.6–0.7 m s^{-1}, yearlong means in excess of 0.10 m s^{-1} and deep eddy kinetic energy of about one quarter of the surface value in the region of maximum variability between the SAF and PF [*Chereskin et al.*, 2009].

[6] The satellite altimetry era brings new perspectives to the monitoring of the ACC circulation and the transport variability through the Drake Passage. For example, *Sprintall* [2003] examined the frequency and propagation paths of eddies between the SAF and PF in DP. *Chouaib et al.* [2006] analyzed the data from two adjacent descending altimetry tracks in DP and showed that the SAF and PF locations were positively correlated whereas their surface transports were strongly anticorrelated. *Barré et al.* [2011] precisely monitored frontal branch locations and identified recurrent flow patterns in DP. The DRAKE project is an attempt to monitor the ACC transport combining current meter data and altimetry, following the successful monitoring the Malvinas transport over long periods [*Spadone and Provost*, 2009]. To achieve this objective, a precise validation of the altimetry in DP is necessary. DP is a stringent test as spatial scales and temporal scales of velocity variations can be short. The DRAKE experimental set up was designed to compare altimetry and in situ data and to use the complementarity between satellite and in situ observations. For this purpose, 10 moorings were deployed in January 2006 in the Drake Passage under track 104 of the Jason satellite and placed at intersections of two Jason tracks. The Jason ground track 104 is located on the eastern side of the Shackleton Fracture Zone, and further to the east than the DRAKE 79 main line moored array [*Hofmann and Whitworth*, 1985]. The ground track passes through the center of the Yaghan Basin. Three years of current and temperature measurements were collected in the Yaghan Basin and two years of data in the Ona Basin.

[7] This paper focuses on the northern part of the Drake Passage where the ACC flow is maximum. We reexamine the circulation in the Yaghan Basin using the three years of new in situ velocity time series gathered at five mooring sites across the Basin and the concomitant altimetric data (Figure 1). A detailed analysis of the current meter data and the comparison with the altimetry-derived surface velocities is a necessary prerequisite before using the 18 yearlong altimetry time series. The in situ data provide the first opportunity to compare the relatively low temporal resolution and large spatial coverage altimetry data with the point measurement high temporal resolution near-surface current meter data in a high kinetic energy environment at high latitudes.

[8] The paper is organized as follows. The data are presented in section 2. The basic statistics and the vertical and temporal structures of the in situ velocity measurements are analyzed in section 3. Exceptional events are noted. Precise comparisons between in situ velocities and surface velocities derived from altimetric data are presented in section 4. The quality of altimetry having been assessed, altimetric data are used, in section 5, to put the in situ point measurements into a spatial context, so as to interpret the principal modes of velocity variation, to place the mooring period into the perspective of the 18 year altimetric data time series and to interpret the events noted in the in situ data in section 3. Finally, results are summarized and perspectives are discussed in section 6.

2. Data

2.1. Current Meter Data

[9] Ten current meter moorings were deployed from R/V *Polarstern* in January 2006 across the Drake Passage [*Provost et al.*, 2011; *Renault et al.*, 2011] The current meter array was anchored under Jason track 104 across the DP (Figure 1). In April 2008, eight moorings were recovered (two of them were lost) and the five northernmost moorings were redeployed and then recovered in March 2009. Three years of current and temperature measurements were made in the Yaghan Basin and two years, in the Ona Basin. The five northernmost moorings, hereinafter referred to as M1–M5 (Figure 1), spanned the Yaghan Basin and are considered in this study. The results from other moorings, across the Ona Basin, are presented in a companion paper [*Ferrari et al.*, 2012]. The array of five moorings comprised 14 current meters (type ANDERAA, MORS and Aquadopp) in 2006–2008 and 15 current meters (type ANDERAA and Aquadopp) in 2008–2009 (Figure 2 and Table 1). Some current meters were placed at the same depth during the first deployment (Figure 2), with an ANDERAA and an Aquadopp (acoustic type) current meter. A careful comparison of these two types was performed [*Kartavsteff*, 2008] and the Aquadopp data were used in the present study. M1 and M3 were equipped with an upward looking acoustic Doppler current profiler (ADCP) incorporated into the uppermost subsurface buoy. Assuming that the vertical shear varies on large vertical scales [*Hofmann and Whitworth*, 1985; *Hughes et al.*, 2003], three current meters on each mooring line were thought to be sufficient to estimate shear variations. M1, M3, M4 and M5 were placed so as to be at the intersections of two Jason tracks. M2 was added midway between M1 and M3 to sample the SAF current core. Unfortunately, mooring M2 could not be recovered in 2008, but was redeployed the same year (Figure 2). Among the 14 current meters successfully brought back, the records on the velocity channels of three current meters ended prematurely in 2006–2008. The ANDERAA and MORS current meters were calibrated for velocity and pressure, before and after deployment, at the Institut Français de Recherche pour l'Exploitation de la Mer (Ifremer). The reported velocity accuracies varied between 1 and 2 cm s^{-1} for the various current meters, with the
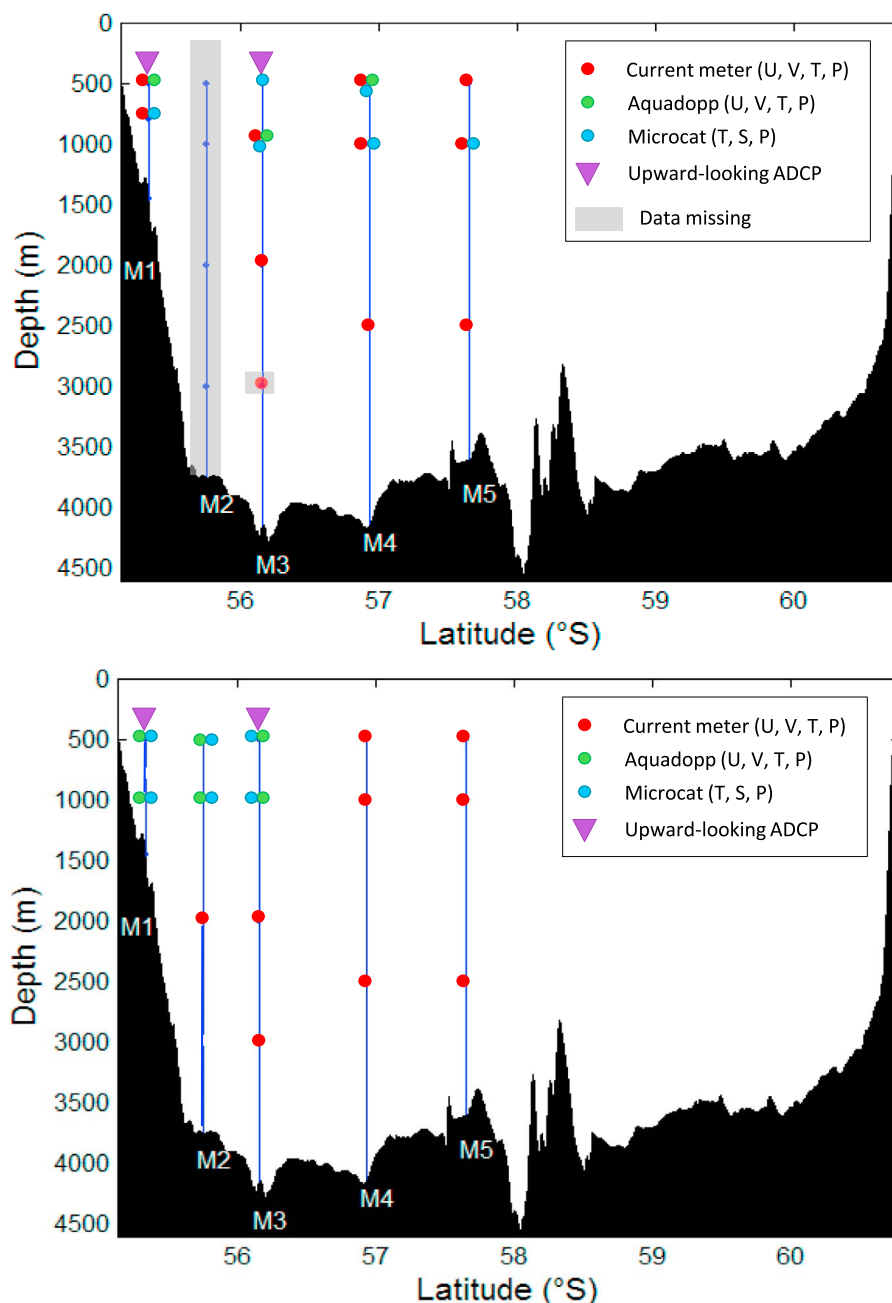
Figure 2. Vertical distribution of the instruments (top) in 2006–2008 and (bottom) in 2008–2009 along the mooring lines. Shaded instruments were lost or malfunctioning. Red dots indicate ANDERAA-type current meters, and green dots indicate Aquadopp-type acoustic current meters. Microcats are indicated by blue dots; the Microcats measure temperature, salinity, and pressure. Purple triangles indicate the position of the moored upward looking acoustic Doppler current profiler (ADCP).

minimum measurable current speeds ranging between 0.53 and 3.78 cm s^{-1}. Velocity data were low-pass filtered, with a cutoff period of 25 h to remove inertial and tidal variations and then resampled at a daily rate.

[10] All instruments experienced vertical displacements during strong current pulses over periods of several days. These displacements were 15–230 dbar (RMS hydrostatic pressure) for the upper instruments, but were smaller at greater depth (Table 1). Largest displacements occurred at moorings M3 and M4, where they exceeded 500 dbars on

the upper current meters about 15 times in 3 years. For M1 and M2, maximum diving events reached 300 dbars for the upper instruments, and 500 dbars for M5–1. A mooring motion-correction scheme adapted from *Cronin and Watts* [1996] was applied, allowing an interpolation (and extrapolation) of the velocity and temperature measurements at fixed depths. Details of this correction method can be found in Appendix A. This correction is important for the estimation of heat fluxes [*Phillips and Rintoul*, 2000] and does not affect much the velocities and the velocity statistics

Table 1a. Vertical Displacements of the Current Meters During the First Period[a]

Mooring	Latitude	Longitude	Depth (m)	Days	Corrected Pressure	Mean Pressure	Minimal Pressure	Maximal Pressure	Standard Deviation Pressure	ΔP
M1-1	55°20′51″S	65°11′15″W	1700	789	60	95	67	440	40	373
M1-2				789	380	404	376	711	35	335
M1-3				434	860	882	855	1076	27	221
M3-1	56°07′92″S	63°42′66″W	4130	812	380	486	368	1487	162	1119
M3-3				812	910	1021	908	1976	155	1068
M3-4				812	1920	1972	1919	2492	74	573
M4-1	56°56′54″S	62°19′61″W	4075	809	430	557	422	1630	189	1208
M4-2				809	960	1085	958	2021	177	1063
M4-3				809	2450	2502	2446	2947	75	501
M5-1	57°37′63″S	60°55′26″W	3325	778	570	614	568	1148	67	580
M5-2				778	1085	1123	1085	1593	56	508
M5-3				778	2645	2653	2645	2745	11	100

[a]The corrected pressure (in dbar) is the nominal pressure taken for the mooring correction and is close to the minimum pressure.

(Appendix A). In the following, corrected velocity and temperature were used.

2.2. Satellite Data

[11] We used two types of altimetric products from the archiving, validation and interpretation of satellite oceanographic data (AVISO) (Collect-Localization-Satellites, CLS Space Oceanography Division): along-track and gridded products (www.aviso.oceanobs.com).

[12] Along-track products from the Jason 1 satellite consist of sea level anomaly (SLA) and absolute dynamic topography (ADT). Values of ADT are obtained by adding the SLA values to the CNES-CLS09 MDT (mean dynamic topography) values. Jason 1 repeats its cycle every 9.9156 d. The noise of the raw along-track SLA is removed using a linear Lanczos low-pass filter with a cutoff at 70 km [*Ducet et al.*, 2000] and the final along-track data are subsampled with a spatial resolution of 18.5 km in DP. M1, M3, M4 and M5 were located at the intersections of two Jason 1 tracks (track 104 and tracks 61, 137, 213 and 35, respectively). Distance between the altimeter crossover points and the mooring locations varied from hundreds of meters to several

kilometers and was largest for the second deployment of M3 with 7142 m (Table 2). Horizontal velocities at each mooring location (except M2) were estimated using the data of the two intersecting tracks. The angles between ascending and descending ground tracks are quite optimal to compute zonal and meridional velocities as they are close to 90° at the latitude of the Yaghan Basin (Table 2). The intersecting tracks are temporally separated by 1.7 d at M1, 1.3 d at M3, 4.3 d at M4 and 2.7 d at M5. No temporal interpolation was performed.

[13] The multisatellite gridded products consist of maps of sea level anomalies (MSLA) with a spatial resolution of 1/3° × 1/3° on a Mercator grid at 7 d intervals; that is, about 20.5 × 20.5 km in the northern part of DP. They are produced by pooling altimetric observations from several satellites (when available): TOPEX/Poseidon or Jason 1; European Remote Sensing Satellite (ERS-1 and -2); Environmental satellite (Envisat); and Geosat Follow-On (GFO) [*Ducet et al.*, 2000]. In addition, we used maps of absolute dynamic topography (MADT), which are the sum of the MSLA and the CNES-CLS09 MDT. Surface geostrophic velocities were derived from these MADT maps. A new MSLA product from AVISO,

Table 1b. Vertical Displacements of the Current Meters During the Second Period[a]

Mooring	Latitude	Longitude	Depth (m)	Days	Corrected Pressure	Mean Pressure	Minimal Pressure	Maximal Pressure	Standard Deviation Pressure	ΔP
M1-1	55°20′16″S	65°11′22″W	1600	345	60	482	473	562	15	89
M1-2				345	490	496	488	577	16	89
M1-3 (653 m)[b]				435	1030	994	988	1061	12	73
M2-1	55°43′13″S	64°24′10″W	3816	343	420	505	418	834	89	416
M2-2				343	930	1002	923	1319	81	396
M2-3				343	2000	2024	1980	2265	50	285
M3-1	56°06′05″S	63°43′93″W	4275	344	300	481	391	1219	115	828
M3-2				344	430	495	405	1234	115	829
M3-3				344	930	1011	928	1707	107	779
M3-4				344	1940	1980	1931	2390	63	459
M3-5 (3706 m)[b]				344	2940	2956	2931	3132	30	201
M4-1	56°55′55″S	62°22′03″W	4093	334	520	669	511	2095	230	1584
M4-2				334	1020	1170	1014	2552	224	1538
M4-3 (3058 m)[b]				334	2540	2648	2531	3583	162	1052
M5-1	57°37′53″S	60°55′01″W	3445	345	520	541	512	891	52	379
M5-2				345	1020	1046	1019	1378	48	359
M5-3 (310 m)[b]				345	2540	2548	2537	2691	21	154

[a]The corrected pressure (in dbar) is the nominal pressure taken for the mooring correction, and is close to the minimum pressure.
[b]Distance in meters between the second deployment mooring location and the first one.

Table 2. Coordinates of Ground Tracks Intersections, Angles Between Ground Tracks, and Distances Between Altimeter Crossover Points and Mooring Locations

Jason 1 Tracks Intersection (Mooring)	Coordinates of Jason 1 Tracks Intersection		Angle Between Jason 1 Ground Tracks	Distance Between Jason Tracks Intersection and Mooring Location (m)	
	Latitudes	Longitudes		2006–2008	2008–2009
104/61 (M1)	55°20′28.2″S	65°11′18″W	87.55°	175	580
- (M2)	-	-	-	-	-
104/137 (M3)	56°9′41.4″S	63°46′12″W	92.23°	4911	7142
104/213 (M4)	56°56′14.4″S	62°21′15″W	92.96°	1749	1502
104/35 (M5)	57°39′6.6″S	60°56′9.6″W	95.65°	2884	3142

with a 1 d resolution, was used to compute the MADT maps and led to no observed changes compared to the 7 d resolution maps. *Barré et al.* [2011] used the MADT to identify the location of frontal branches, major meanders and eddies during the deployment cruise in 2006 and this proved particularly valuable for the interpretation of the in situ data.

3. Current Meter Observations

3.1. General Description

[14] The zonal and meridional velocity components are presented in Figure 3 for the entire observing period (January 2006–April 2008 and April 2008–March 2009). There are three levels per mooring, except for M3, at which currents are shown at four different depths (300, 500, 1000 and 2000 m). One bin of the upward looking ADCPs is shown at 60 m depth for M1-1 and at 300 m depth for M3-1. These two levels, 60 m for M1-1 and 300 m for M3-1, were chosen for being the only bin continuously measured during the two periods. At each mooring, the three measurement levels showed a vertical consistency in the velocities. The standard deviation ellipse axes and mean velocity vectors (Figure 4 and Table 3) were roughly parallel at the three levels for each mooring.

3.1.1. Mooring 1

[15] M1 was located on the steep part of the South American continental slope above the 1550 m isobath (Table 1). The direction of the mean flow was oriented northeastward, parallel to the isobaths, and standard deviation ellipses were stretched in the same direction (Figure 4). Maximum velocities at 60 m depth reached 90 cm s^{-1} (February 2007) and 70 cm s^{-1} at 400 m depth (January 2007) (Figure 3). Mean velocities were higher during austral summer and autumn, with a mean eastward velocity of 23 cm s^{-1} at 60 m depth and 19 cm s^{-1} at 400 m depth, between January and June, than during winter and spring, with a mean eastward velocity of 11 cm s^{-1} at 60 m depth and 10 cm s^{-1} at 400 m depth, between July and December. Reversals of the flow were rare, but could be associated with high velocities, as in July 2006 and in January 2007, with a southwestward velocity of 75 cm s^{-1} at 60 m depth. In November 2006, the flow remained oriented southwestward during the entire month at all depths. This event is described in section 5.3. The amplitude and direction of the mean velocities and standard deviation ellipses were consistent between the two periods, a noticeable difference being that the standard deviation ellipses at the two deeper levels were larger during the first period than during the second (Table 1).

3.1.2. Mooring 2

[16] One year of data (2008–2009) was available for mooring M2, which was located at the bottom of the continental slope, above the 3800 m isobath. Mean velocities, ranging from 37.7 cm s^{-1} at 500 m depth to 11.8 cm s^{-1} at 2000 m depth, were northeastward (Figures 3 and 4). Velocities at 500 m depth were high, with a mean amplitude of 37.7 cm s^{-1}, and frequently exceeded 60 cm s^{-1}, reaching a maximum of 102 cm s^{-1} (end of July 2008). The mean velocity of 23.6 cm s^{-1} at 1000 m depth was the highest mean velocity measured at that level in the whole array. Moreover, the mean velocities at M2 were remarkable compared to those at the other moorings, as they were twice as great as the standard deviation ellipse axes (Table 3). The major axis of the ellipses (Figure 4) was oriented west to east at all depths, in agreement with the fact that the flow is stronger when parallel to the isobaths and weaker when going toward the continental slope. A few reversals of the flow were noticed, with a northwestward flow at all depths (Figure 3), greater in April–May 2008 and smaller in October 2008 and January 2009. The April–May 2008 situation is discussed in section 5.3.

3.1.3. Mooring 3

[17] M3 was located in a deep part of the Yaghan Basin, the Yaghan seafloor depression (YSD) (4200 m), downstream of the Yaghan seamounts (YS) which culminate at 1500 m below the sea surface (Figure 1b). M3 was the most instrumented mooring, with an upward looking ADCP, sampling from 450 to 200 m depth, current meters at 1000 and 2000 m depth during three years (2006–2009), and two additional current meters in 2008–2009, at 500 and 3000 m depth (Figure 2). The mean flow at M3 was oriented north-northeastward and was high from surface to bottom. Velocities at 300 m depth reached a maximum of 90 cm s^{-1} in May 2008, while the mean velocity at this depth was only 22.5 cm s^{-1}. At 2000 and 3000 m depths, maximum velocities exceeded 40 cm s^{-1} and the mean velocities were 11.2 and 12.7 cm s^{-1}, respectively (Table 3). The flow reversed from east to west quite often from top to bottom (Figure 3). A major reversal in the north–south component occurred in late July 2008, with a southward component reaching 60 cm s^{-1}; it is discussed in section 5.3. The two measurement periods provided similar mean velocities and major ellipse axes (Table 3). At 3000 m depth (2008–2009), the standard deviation ellipse, with a major axis smaller than the mean velocity, was stretched in the direction of the mean flow (north-northeastward), because of a bathymetric constraint (Figure 1c). The slight counterclockwise veering of
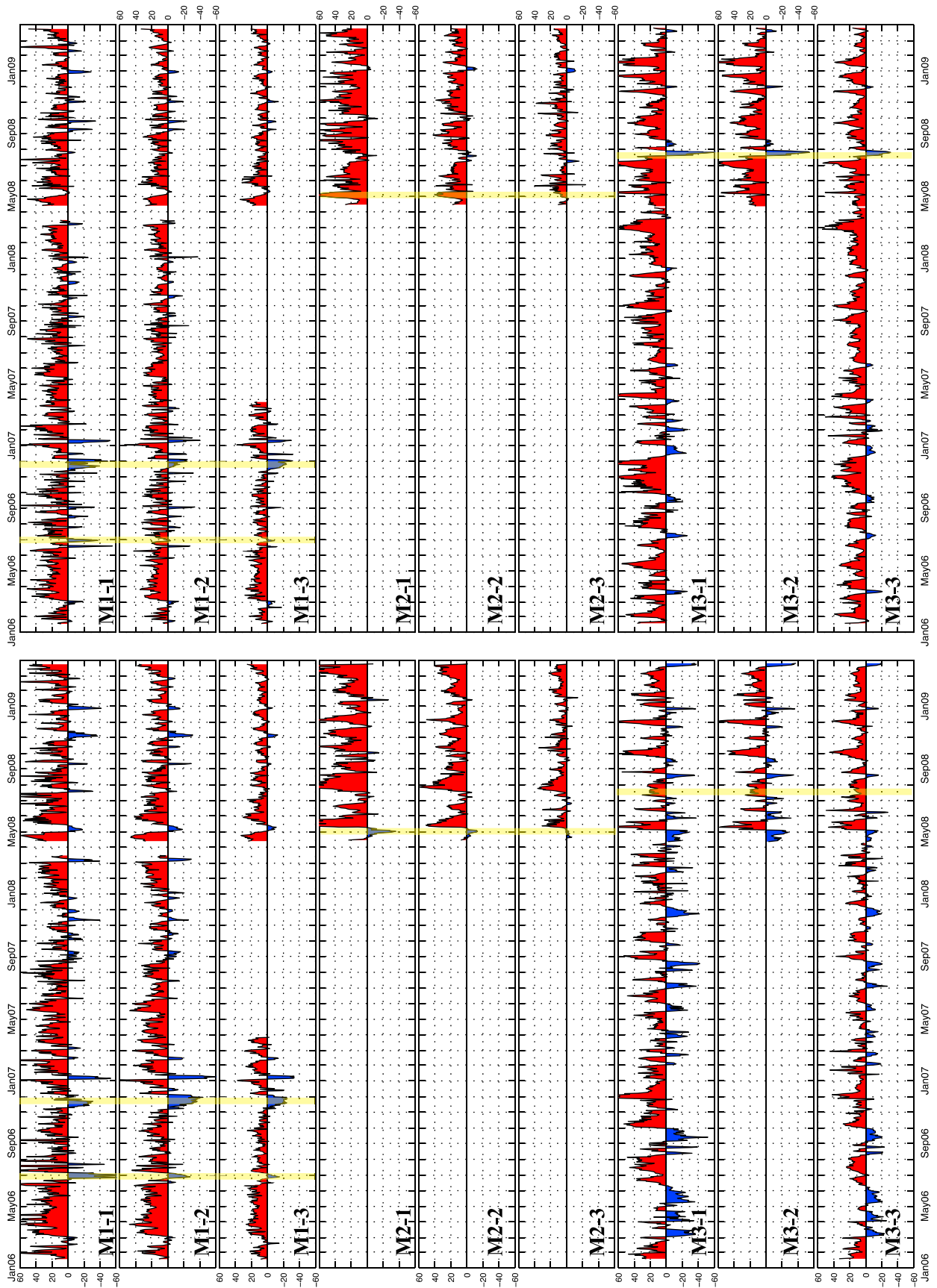
Figure 3

the mean velocity vectors with depth, below 500 m, was consistent with a mean downwelling induced by the increasing sea depth in the YSD past the upstream obstacle of the YS.

3.1.4. Mooring 4

[18] M4, with a westward component in the mean velocity at all depths and for both observation periods, 2006–2008 and 2008–2009 (Figure 4) stood out. The amplitude of the mean velocity vector increased with depth while the length of the axes of the standard deviation ellipses decreased. At 1000 m depth, the flow was westward most of the time, and the u component reversed less often than at 500 m depth and more often than at 2500 m depth (Figure 3). Except in June and July 2006, when the flow was eastward and reached 20 cm s^{-1}, velocities at 2500 m depth were mostly westward (Figure 3), reaching amplitudes of 40 cm s^{-1} on ten occasions over the three years. The mean velocity at 2500 m depth was consistent between the two periods: 13.2 cm s^{-1}, 81°W, for 2006–2008 and 14.0 cm s^{-1}, 79°W, for 2008–2009 (Table 3). It was higher than the mean velocity at 500 m depth (7.0 cm s^{-1} and 10.2 cm s^{-1} for the two periods, respectively) and exceeded the length of the standard deviation ellipse axes (Figure 4). The direction of the mean velocity was rotated by 40° to the west at 500 m depth (and by 20° at 1000 m depth), between the first and second periods. Standard deviation ellipses were larger during the first period than during the second, indicating a higher variability (Table 3). The period from June to August 2006 stood out as a period of particular interest: velocities were eastward at all depths, reaching 60 cm s^{-1} at 500 m and 1000 m depths, and 40 cm s^{-1} at 2500 m depth (Figure 3). This period is examined in section 5.3.

3.1.5. Mooring 5

[19] Mooring M5 was located at the northern exit of a valley oriented northwest–southeast and transverse to the WSR (Figure 1c). The mean velocity at M5 was northeastward during 2006–2008 and eastward in 2008–2009 throughout the water column (Figure 4). Mean velocities were greater than the standard deviation ellipse axes, but were not as great as the mean velocities at M2. The mean velocity at 500 m depth in 2006–2008 was 21.5 cm s^{-1}, whereas the ellipse axes were 18.3 cm s^{-1} and 15.7 cm s^{-1} (Table 3). The standard deviation ellipses were oriented from northwest to southeast parallel to the direction of the valley and stretched out with depth. Velocities reached a maximum of 73 cm s^{-1} at 500 m depth at the end of March 2006. Few westward flows were noticed at 500 m and 1000 m depth during 2006–2009 and were usually of small amplitude (less than 20 cm s^{-1} at 500 m depth). At 2500 m depth, the flow was of small amplitude, with peak values seldom reaching 20 cm s^{-1} and with a mean velocity of 3.2 cm s^{-1} during the first period and 5.4 cm s^{-1} during the second period.

[20] In summary, a notable feature was the mean velocities with a westward component in the center of the Yaghan

Basin, at M4, whereas, as expected, mean eastward velocities were observed for all other moorings. The persistent westward velocities at depth at M4, with a mean westward velocity greater than the standard deviation ellipse axis, suggested a permanent deep cyclonic circulation in the Yaghan seafloor depression (Figure 1b), with the shallow topography to the left of the current direction, as expected in the southern hemisphere.

[21] Globally, the statistics for the two measurement periods were similar. However, differences between the two periods were observed both in the means and the standard deviation ellipses. At M5, during the first period, the amplitude of the mean velocity was 5.4 cm s^{-1} greater than during the second period and the mean current was more than 40° further north than during the second period. Standard deviation ellipses at depth were larger at M1 during the first deployment than during the second etc. These differences are analyzed and interpreted in section 5.2, using altimetry.

3.2. Vertical Structure of the Velocity Variation

[22] A principal component analysis was performed on the velocities, considering each mooring and the two periods separately, to provide a quantitative overview of the vertical structure of the velocity variation. The three leading empirical orthogonal functions (EOF) explained between 92.9% and 98.2% of the variability (Figure 5) for each of the five moorings over the two periods. The first EOF accounted for 44.7–75.8% of the total variance, while the second EOF explained 16.3–39.7% of the variance (Figure 5). At M1 and M2, the first EOF explained a large fraction of the variance: over 72% at M1 and 61.2% at M2. The third EOF explained a larger fraction of the variance near the continental slope (close to 9% at M3) than in the center of the Yaghan Basin (between 2.2% and 3.1% at M4 and M5).

[23] At each mooring, the directions of the first two EOF vectors were identical to the directions of the axes of the standard deviation ellipses except when the standard deviation ellipses were close to circular like at M3 and M4 for the period 2006–2008. For the first and second EOFs, the directions of the vectors did not vary with depth and the amplitudes of the vectors decreased with depth, indicating an equivalent barotropic vertical structure. The third EOF corresponded to a baroclinic component.

[24] At M1, the first EOF parallel to the mean flow could be interpreted as acceleration or a deceleration of the flow (with more than 72% of the explained variance) and the second EOF to a change of direction (upslope/downslope – 20% of the standard deviation ellipse). The third EOF (which explained less than 4.7% of the variance) changed sign between 60 m and 500 m depths.

[25] At M2, the variability of the flow occurred principally in a direction parallel to the isobaths west to east (61.2% of the variance for the first EOF), and less in the direction of the second EOF, south to north direction (28.4% of the variance; Figures 4 and 5). The baroclinic

Figure 3. Time series of velocities (in centimeters per second) from January 2006 to April 2009 for Moorings M1-1 to M5-3. The u (west-east) component is shown in the left panel and the v (south-north) component in the right panel. Three instruments per mooring are shown, except for M3, where four instruments are plotted. Positive velocities are shaded in red, and negative velocities are shaded in blue. Vertical yellow lines indicate the exceptional events studied in section 5.3.
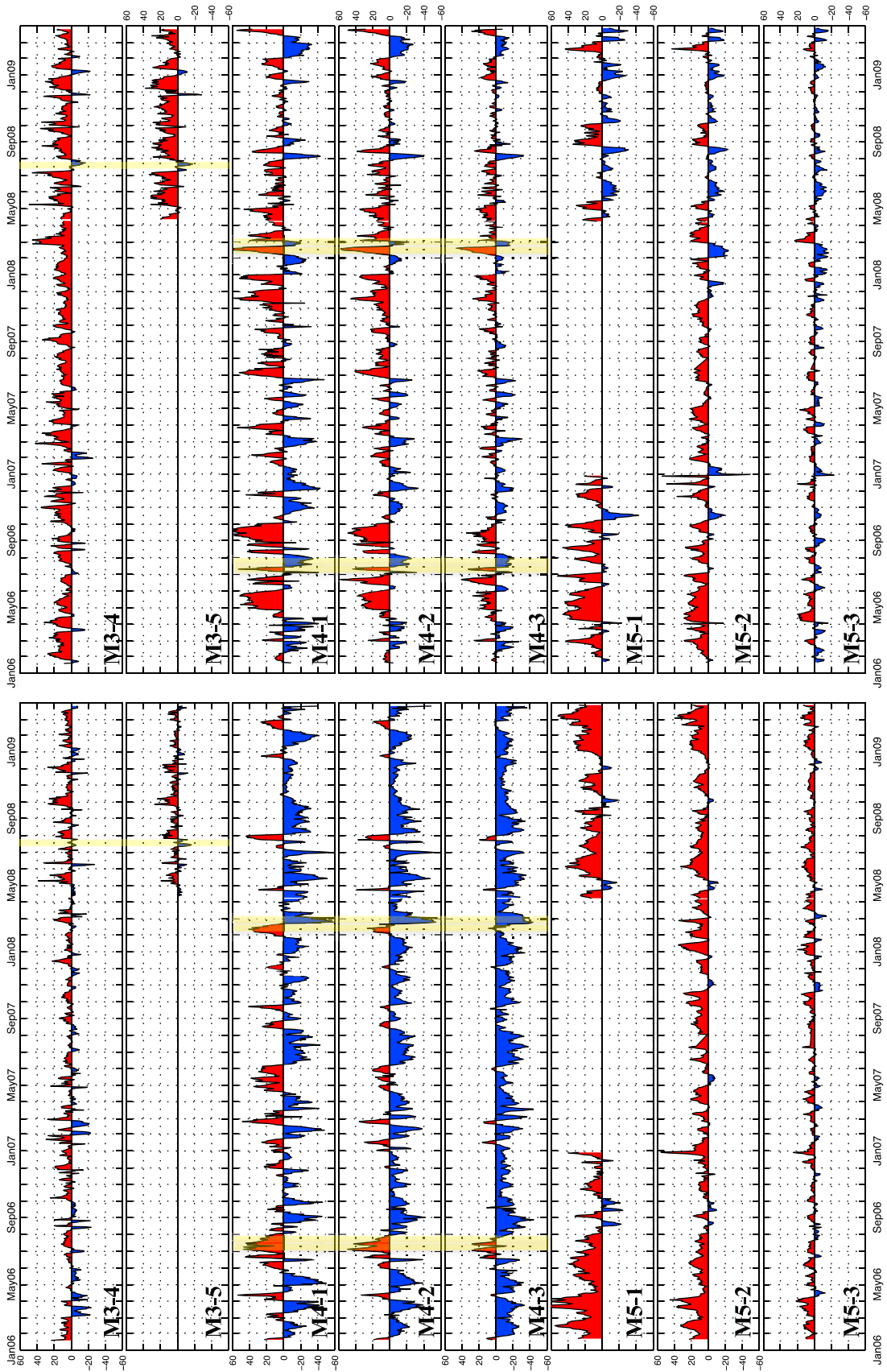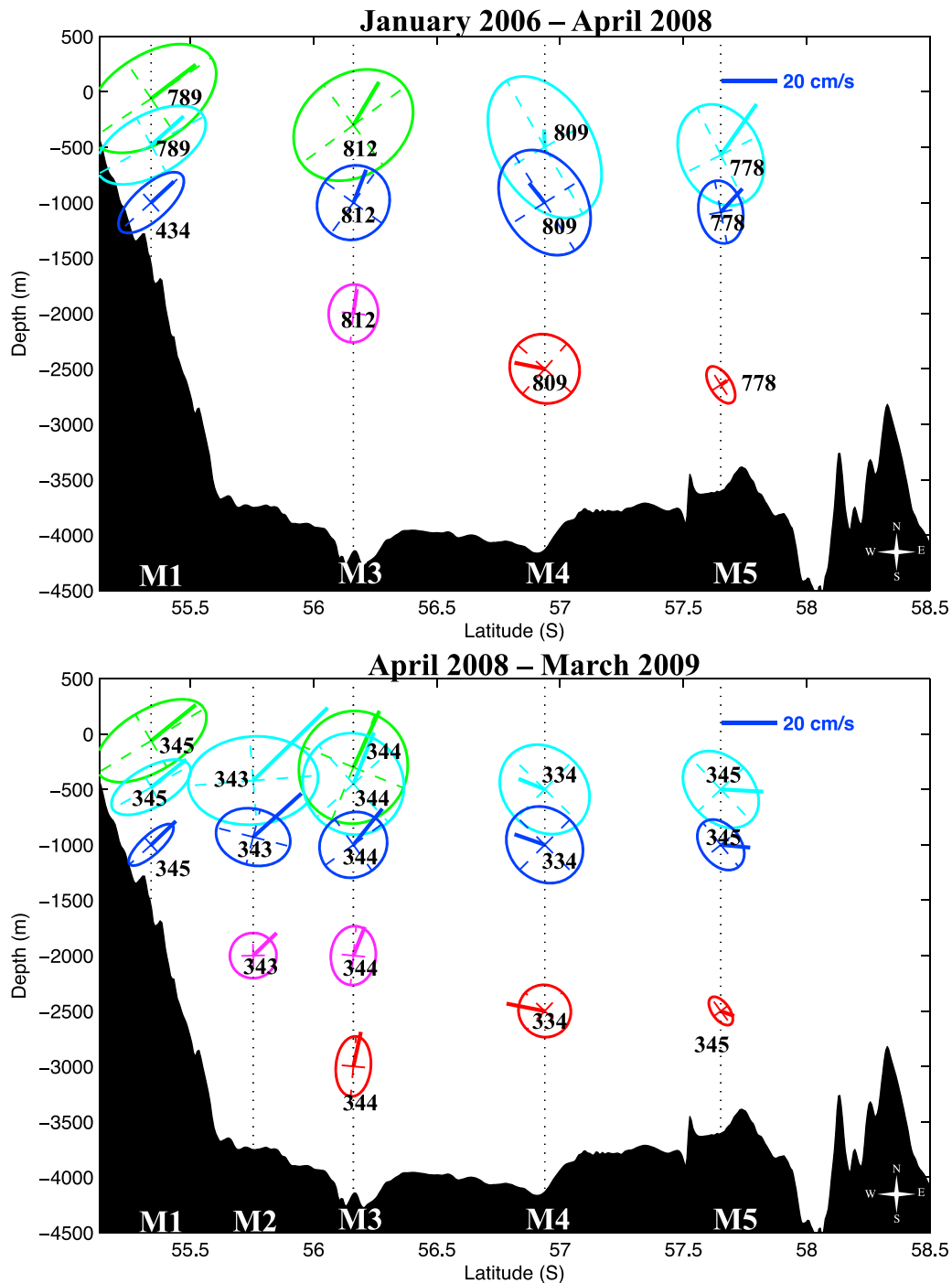
Figure 3. (continued)

Figure 4. Mean velocities and variance ellipses for (top) the first period, 2006–2008, and for (bottom) the second period, 2008–2009. The number of days of measurement is indicated in black. The axes of the ellipses are plotted in a thin dotted colored line. Ellipses corresponding to the level of the upward look-ing ADCP (60 m for M1-1 and 300 m for M3-1) are plotted in green. Ellipses at 500 m depth are plotted in cyan at 1000 m depth, in blue at 2000 m depth, in magenta at 2500 m depth, in red (M4 and M5), and at 3000 m depth (M3), also in red. Bottom topography is in solid black.

component, shown by the third EOF, changed sign between 300 and 900 m depths and explained 5.3% of the variance.

[26] At M3, during the first period (2006–2008), when three current meters were available, the first EOF, explaining 51.8% of the variance, was oriented northeastward, in the direction of the mean flow (Figures 4a and 5a) and parallel

to the major axes of the standard deviation ellipses. The second EOF accounted for 37.9% of the variance. The third EOF (4.7% of the variance) changed sign between 500 and 1000 m depths. During the second period, 2008–2009, five instruments sampled the water column, with two of them close to each other, at 300 and 500 m depths. Several EOF

Table 3a. Statistics of the Mooring Data for the First Period[a]

Mooring	Reference[b]	Days	Mean Pressure	Mean Norm (cm s^{-1})	Angle of Mean Norm (deg)	Standard Deviation Norm	Major Axis (cm s^{-1})	Minor Axis (cm s^{-1})
M1-1	ADCP	789	60	20.4	51.2	15.6	22.6	12.9
M1-2	AA	789	380	16.5	50.6	11.5	18.5	9.4
M1-3	AA	434	860	11.6	48.1	8.6	14.4	6.0
M3-1	ADCP	812	380	19.2	25.5	15.7	20.8	17.1
M3-3	AA	812	910	14.2	17.9	9.5	12.5	11.4
M3-4	AA	812	1920	10.6	9.1	7.5	9.4	7.8
M4-1	AA	809	430	7.0	−24.7	14.8	23.3	18.8
M4-2	AA	809	960	10.4	−48.0	12.1	16.9	14.2
M4-3	AA	809	2450	13.2	−81.3	8.9	11.6	11.0
M5-1	MO	778	570	21.5	50.9	14.0	18.3	15.7
M5-2	AA	778	1085	12.2	52.8	8.4	10.5	8.9
M5-3	AA	778	2645	3.2	85.0	4.5	7.8	4.1

[a]Major axis and minor axis are the lengths of the standard deviation ellipse axes. Angles are in degrees (°), pressures are in decibar and velocities are in centimeters per second.
[b]AA, ANDERAA-type current meter; ADCP, acoustic Doppler current profiler; MO, MORS-type current meter.

analyses were performed using different numbers of instruments. With three instruments (at 300, 1000 and 2000 m depths), the results were identical to those obtained in the first period. When considering four instruments in the vertical (Figure 5), by including the instrument at 3000 m depth, the first, second and third EOFs explained, 44.7%, (with a direction close to south–north), 39% and 9.1%, respectively, of the total variance. The third EOF was oriented parallel to the first EOF for the two lower instruments and was bottom intensified, being greater than the first EOF for the lowest instrument.

[27] At M4, the EOF analysis was consistent over the two periods: same percentage of explained variance, same structure and the rotation of the EOF vectors being consistent with the standard deviation ellipses (Figure 5). The first EOF was northwestward and had the same direction as the mean flow. The third EOF, a baroclinic component changing sign between 500 and 1000 m depths, explained less than 3.1% of the variance.

[28] At M5, the first EOFs, explaining 52.4% and 64.6% of the variance for the periods 2006–2008 and 2008–2009,

respectively, was oriented northwestward, nearly perpendicular to the mean velocities (Figures 4 and 5). This was coherent with the standard deviation ellipses and the seafloor topography: the first EOF, which was parallel to the major axes of the standard deviation ellipses, indicated preferential variation along the axis of the transverse valley. The third EOF was small (2.9% and 2.2% for the two periods, respectively), followed the direction of the transverse valley at 2500 m depth and changed sign between 500 m and 1000 m depths.

3.3. Temporal Scales

[29] We examined the temporal scales present in the 3 yearlong time series associated with the three first EOFs (Figure 6). To produce these 3 yearlong time series, the problem of missing data at M1, M3 and M5 had to be dealt with.

[30] At M1, the lower instrument (1000 m depth) provided no data between April 2007 and March 2008. An EOF analysis was performed with three current meters over the period 2006–2007 and with two current meters over the period 2006–

Table 3b. Statistics of the Mooring Data for the Second Period[a]

Mooring	Reference[b]	Days	Mean Pressure	Mean Norm (cm s^{-1})	Angle of Mean Norm (deg)	Standard Deviation Norm	Major Axis (cm s^{-1})	Minor Axis (cm s^{-1})
M1-1	ADCP	345	60	20.7	51.1	16.6	22.4	11.1
M1-2	AA	345	490	16.1	51.7	11.1	15.9	7.2
M1-3	AA	435	1030	12.3	46.2	8.6	10.4	3.6
M2-1	Aq	343	420	37.7	45.8	19.7	23.5	15.9
M2-2	Aq	343	930	23.6	48.0	10.8	13.6	10.2
M2-3	AA	343	2000	11.8	46.2	8.1	8.4	8.2
M3-1	ADCP	344	300	22.5	24.8	17.1	20.5	19.5
M3-2	Aq	344	430	20.2	22.3	14.6	18.7	17.7
M3-3	AA	344	930	16.9	39.3	11.2	11.4	12.5
M3-4	AA	344	1940	11.2	22.1	8.6	10.7	8.1
M3-5	AA	344	2940	12.7	12.7	8.0	10.9	6.3
M4-1	AA	334	520	10.2	−67.7	12.5	17.5	14.7
M4-2	AA	334	1020	11.5	−70.7	10.9	14.8	12.8
M4-3	AA	334	2540	14.0	−79.1	7.9	9.7	9.3
M5-1	AA	345	520	15.4	93.0	11.3	14.8	11.4
M5-2	AA	345	1020	10.7	95.5	7.7	10.2	7.1
M5-3	AA	345	2540	5.1	110.8	4.3	6.0	3.1

[a]Major axis and minor axis are the lengths of the standard deviation ellipse axes. Angles are in degrees (°), pressures are in decibar and velocities are in centimeters per second.
[b]AA, ANDERAA-type current meter; ADCP, acoustic Doppler current profiler; Aq, Aquadopp-acoustic type current meter; MO, MORS-type current meter.

Table 3c. Statistics of the Mooring Data for the 3 Year Period[a]

Mooring	Days	Mean Pressure	Mean Norm (cm s^{-1})	Angle of Mean Norm (deg)	Standard Deviation Norm	Major Axis (cm s^{-1})	Minor Axis (cm s^{-1})
M1-1	1134	60	20.5	51.2	15.9	22.5	12.3
M1-2	1134	380	16.4	50.9	11.54	17.7	8.8
M1-3	869	860	12.0	47.3	8.7	12.8	5.1
M2-1	343	420	37.7	45.8	19.7	23.5	15.9
M2-2	343	930	23.6	48.0	10.8	13.6	10.2
M2-3	343	2000	11.8	46.2	8.1	8.4	8.2
M3-1	1156	300	20.9	25.3	16.2	20.7	18.0
M3-2	344	430	20.2	22.3	14.6	18.7	17.9
M3-3	1156	930	14.7	14.9	10.1	12.7	11.6
M3-4	1156	1940	10.7	13.0	7.9	9.8	8.0
M3-5	344	2940	12.7	12.7	8.0	10.9	6.3
M4-1	1143	430	7.5	−41.3	13.5	21.3	18.1
M4-2	1143	960	10.6	−55.4	11.2	15.9	14.1
M4-3	1143	2450	13.5	−80.5	8.4	10.9	10.3
M5-1	1123	570	17.1	68.9	13.3	18.1	14.5
M5-2	1123	1085	11.0	64.7	7.9	10.7	8.1
M5-3	1123	2645	3.7	95.7	5.1	7.2	3.6

[a]Major axis and minor axis are the lengths of the standard deviation ellipse axes. Angles are in degrees (°), pressures are in decibar and velocities are in centimeters per second.

2008. The first three EOFs based on the respective time series were similar during 2006–2007, whether they were produced with the data from two or from three current meters. The third EOF changed sign between 60 m and 500 m depths in both cases. Therefore, only the time series obtained for the two upper current meters over the 3 year period were considered in the following, but the vertical structure over the three current meters is shown.

[31] At M3, during the second observation period (2008–2009), five current meters were available in the vertical. As seen in the previous section, adding the lowest current meter (at 3000 m depth) increased the explained variance of the third EOF from about 5% to about 9.1%. Consequently, for the sake of consistency over the two periods, the time series obtained with three current meters in the vertical (300 m, 1000 m and 2000 m depths) over the three years were taken into account in the following.

[32] At M5, the upper current meter (at 500 m depth) was missing data between January 2007 and March 2008. In contrast to M1 and M3, the data at 500 m depth were essential for a comparison with the surface velocities derived from altimetry (next section). Thus, a combination of the EOF vertical structure and the associated time series was used to estimate missing data at 500 m depth between January 2007 and March 2008. When comparing the EOF analysis performed over one year (2006–2007) with three current meters and that performed over two years (2006–2008) with two current meters, the three first EOFs explained 97.7% of the total variance in both cases, and the spatial structure and the associated time series when available were similar. Using the similarity of the EOF analyses based on two or on three current meters, velocities at 500 m depth were interpolated during the period when data were missing: the EOF vectors from the analysis using three current meters were computed with the time series of the first three EOFs of the analysis using two current meters for the period 2006–2008. The results were compared to the in situ data for the period 2006–2007, and the computed velocities were found to be close to the in situ data (RMS difference less than 3 cm s^{-1}). The velocities at 500 m depth computed by this method

during the period when data were missing were used in the following.

[33] A wavelet analysis was performed on the time series associated with each EOF (Figure 6) over the 3 year period (2006–2009), considering the current meters at similar depths for the two periods. Peaks over the 95% confidence level in the global wavelet spectrum (not shown) were considered as significant and are discussed below.

[34] At M1, the time series of the first mode (oriented in the direction of the mean flow) showed a clear annual cycle with an amplitude of 40 cm s^{-1} (Figure 6): the mean flow was weaker from July to December (11 cm s^{-1} at 60 m depth), and stronger from January to June (23 cm s^{-1} at 60 m depth). If the structure of the first EOF was barotropic equivalent, the second EOF showed a clockwise rotation with depth associated with energy peaks at periods from 5 to 15 d. This range of periods, which corresponds to the frequency of coastal-trapped waves (CTW) [*Brink*, 1991], was significant in the time series of the second EOF. The CTWs were more energetic from June 2006 to March 2007, they did not show any seasonality and did not seem linked to the annual period of the first EOF. An 8–10 d frequency was present at M2 associated with the second EOF, with less energy, indicating the offshore decay of the CTWs. However, measurements of M2 were available only for the period 2008–2009, when the 5–15 d period was less energetic at M1. The greater CTW activity during the first deployment than during the second was reflected in the larger ellipses at depth at M1 during the first period (Figure 4).

[35] In contrast, at M2, M3, M4 and M5, high energy was found in the first, second and/or third EOF at periods from 15 to 60 d, which correspond to the periodicity of mesoscale activity, such as eddies and meanders, at high latitudes. The first EOF was parallel to the mean flow, except for M5, where the second EOF was. The EOF oriented along-flow showed energetic periods, ranging from 20 to 30 d at M2, M3 and M4 and, with less energy, at M5. The second EOF, oriented perpendicularly to the mean flow (for M5, the first EOF), showed a large range of significant periods at M3, M4 and M5: from 15 to 40 d, with a higher energetic peak at
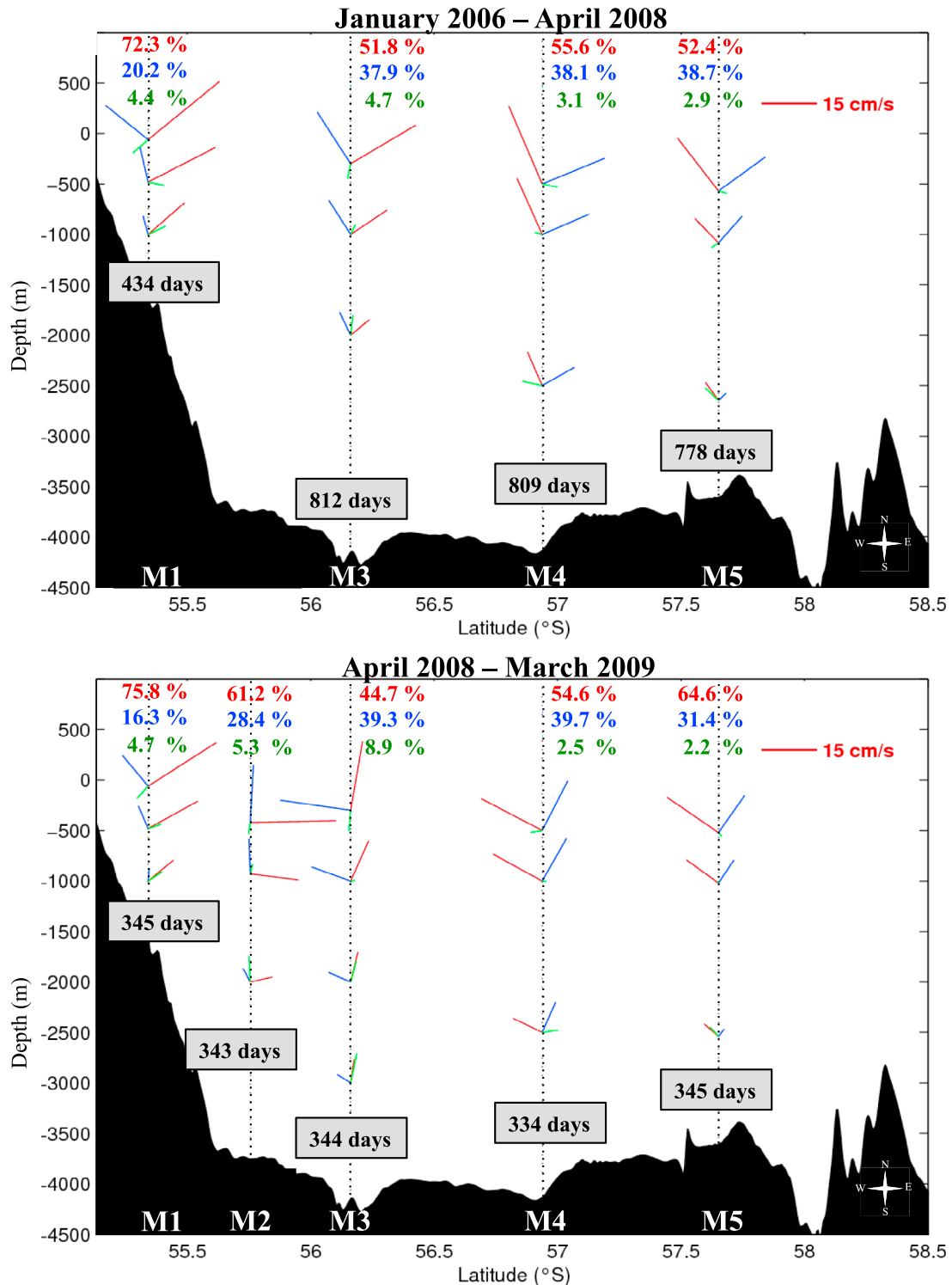
Figure 5. Empirical orthogonal functions (EOF) analysis of (top) the first period, 2006–2008, and of (bottom) the second period, 2008–2009. The first three EOFs for each mooring are plotted at the corresponding depths and latitude. The first EOF is plotted in red, the second in blue, and the third in green. The explained variance of each EOF is indicated by the corresponding color at the mooring position and the number of days of measurement in black. The bottom topography is indicated in solid black. Velocity scale is indicated in the upper right corner and compass directions in the lower right corner. The EOF analysis shown for M3 in the second period was performed with four instruments instead of five (i.e., without M3-2 at 500 m depth) to ensure coherence with the first period.
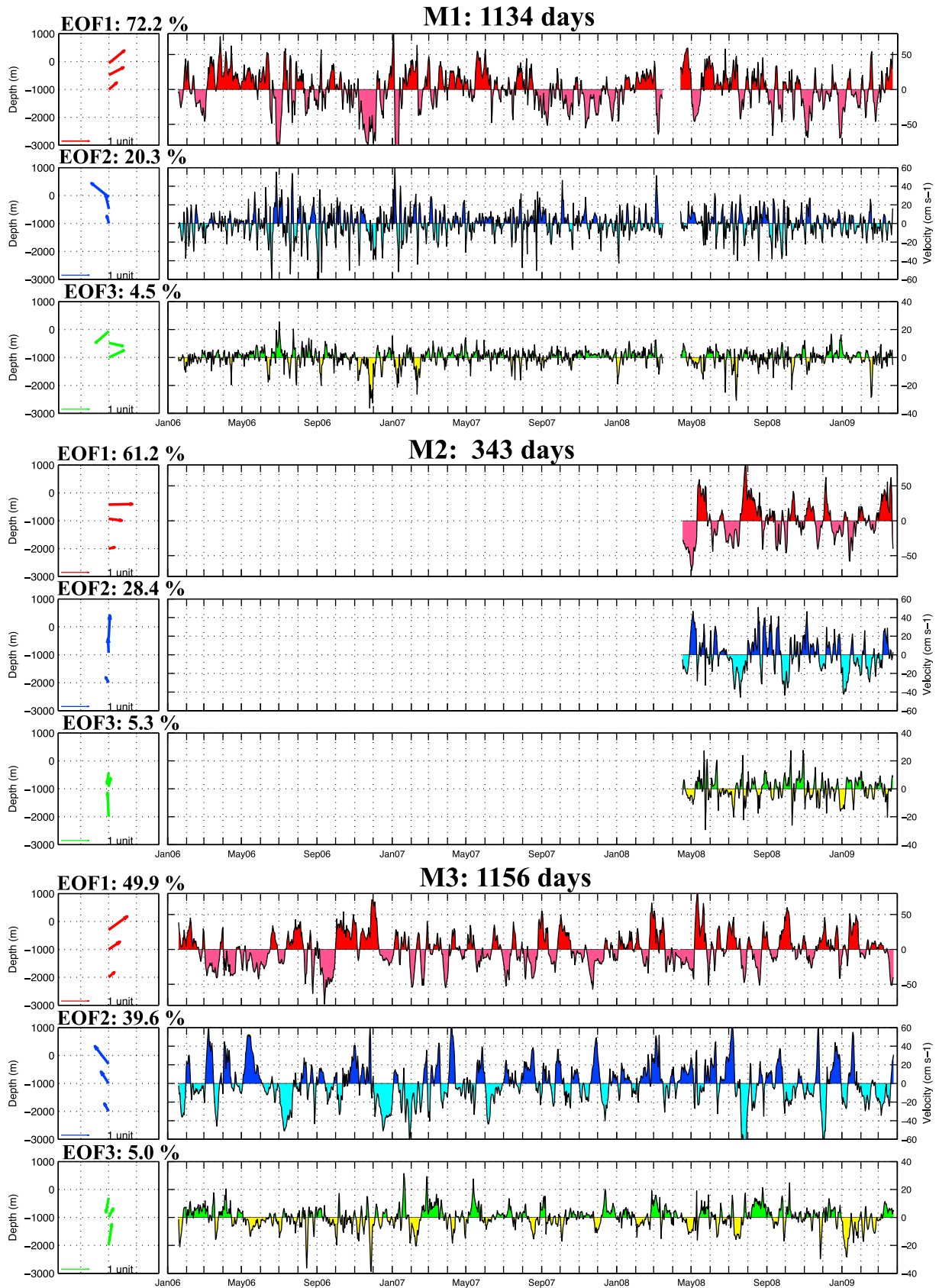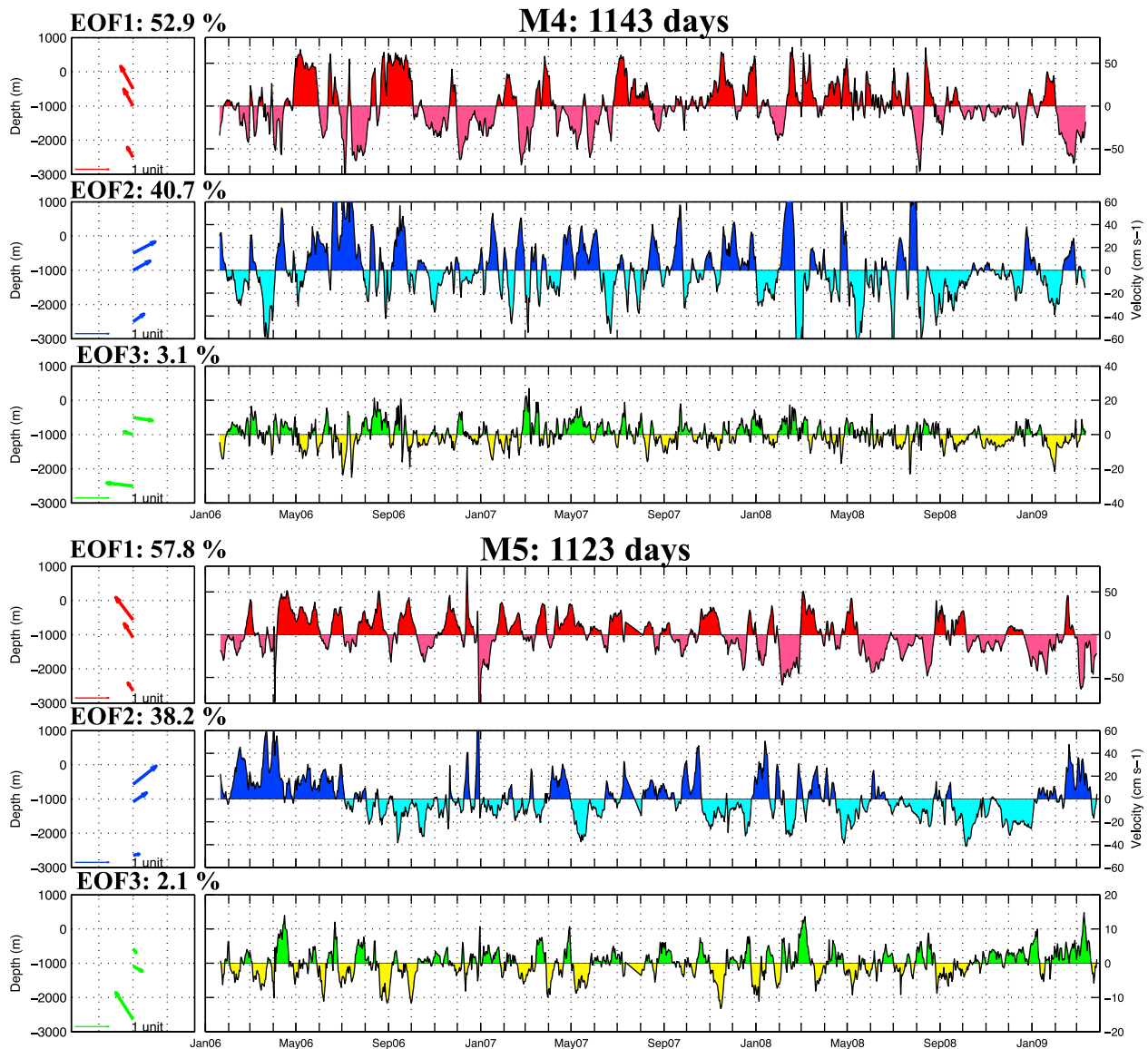
Figure 6

Figure 6. (continued)

35 d. At M2, high energy was observed at periods of 20–25 d in the third EOF (5.3% of the explained variance), which indicated the baroclinic component. At M3 and M4, the third EOF (respectively 5% and 3% of the explained variance) showed an energetic period of 64 d and of 40 d for M5 (6.2% of the explained variance).

4. Satellite-Derived Surface Geostrophic Velocities at the Mooring Sites

[36] The EOF analysis performed on each mooring showed that, globally, the velocity variation had an equivalent barotropic vertical structure. The objective of this section is to compare surface velocities computed from maps of absolute dynamic topography (MADT) and from Jason 1 track data to the in situ data (Figures 7, 10, and 11).

4.1. Means and Standard Deviation Ellipses of Altimetrically Derived Surface Geostrophic Velocities

[37] Mapped surface geostrophic velocities (MSGV) computed from MADT and from Jason 1 track data (JSGV) were averaged over the sampling period of the upper current meter at each mooring location (Table 4).

[38] Mean surface velocities derived from altimetry and mean in situ velocities had comparable directions (within

Figure 6. EOF analysis of the 3 year period (2006–2009) for moorings M1, M2, M3, M4, and M5. For each mooring, the three first EOFs (left column) and the corresponding time series (right column) are shown. Colors are the same as for Figure 5: EOF 1 is plotted in red, EOF 2 in blue, and EOF 3 in green. The explained variance for each EOF is given on the left, and the number of days over which the analysis was done is indicated over each mooring.
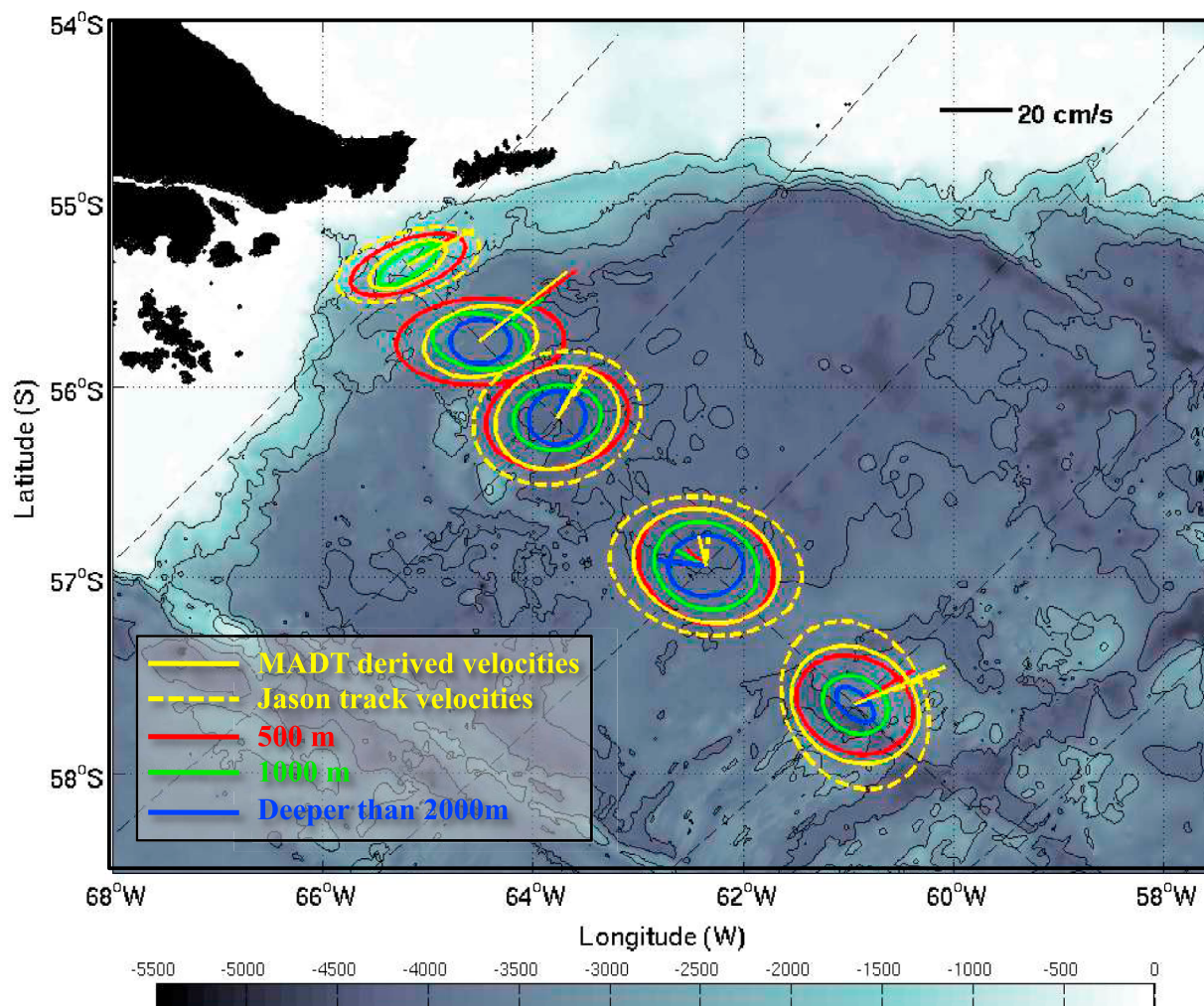
Figure 7. Mean and variance ellipses of the altimetrically derived surface velocities and the in situ velocities over the 3 year period: from 21 January 2006 to 1 April 2009. Surface velocities derived from maps of absolute dynamic topography (MADT) are shown by solid yellow lines and those derived from Jason 1 track data are shown by dashed yellow lines. M2 is not at an intersection of two Jason tracks and therefore no velocities have been computed from Jason 1 track data. Means and ellipses at different depths of the in situ velocities are plotted in red for 500 m depth, green for 1000 m depth, and blue for depths greater than 2000 m. Time resolution is 1 d for in situ velocities, 7 d for MADT-based velocities, and 10 d for Jason 1 track-based velocities. Bottom topography as in Figure 1.

less than $10°$) at all moorings except M4, where the direction of the mean MSGV was rotated clockwise by $33.6°$ and the mean JSGV by $45.4°$, with respect to the mean velocity at 500 m depth (Figure 7 and Table 4). The time lag of 4.3 d between the two Jason tracks intersecting at M4 (section 2.2) could be a reason for the differences in the direction of the mean MSGV and the mean JSGV there. The direction of the mean MSGV at M4 was consistent with the counterclockwise veering with depth observed in the mean in situ velocities.

[39] The mean MSGV (JSGV) exceeded the mean in situ velocity at 500 m depth by 5 cm s^{-1} (6.1 cm s^{-1}) for M1; 0.1 cm s^{-1}, for M2; 3.5 cm s^{-1} (2.6 cm s^{-1}), for M4; and 10.2 cm s^{-1} (9.2 cm s^{-1}), for M5. At M1, the difference reduced to 0.9 cm s^{-1} (MSGV) and 2 cm s^{-1} (JSGV) when compared to the mean in situ velocity at 60 m depth. At M3, the mean MSGV and JSGV were smaller than

the mean in situ velocity at 500 m depth by 0.3 cm s^{-1} and by 4.3 cm s^{-1}, respectively. From the hydrographic data collected in 2006 on track 104, the difference between geostrophic velocity at the surface and 500 m was 5 cm s^{-1} [*Renault et al.*, 2011]. This suggested that the mean MSGV at M5 was overestimated by 4 cm s^{-1} and that the mean MSGV at M2 and M3 were underestimated by about 5 cm s^{-1}. Note that the mean MSGV (JSGV) exceed the in situ velocities at 60 m at M1 by only 1 cm s^{-1}.

[40] Variances computed from JSGV were higher than those obtained from the in situ velocities at 500 m depth for all moorings (M1, M3, M4 and M5). The major axes of the standard deviation ellipses computed using the JSGV were larger, by 3.8 cm s^{-1} (M1) to 11.7 cm s^{-1} (M5), than the major axes of the standard deviation ellipses of the in situ velocities at 500 m depth. In contrast, variances computed from MSGV were lower than variances computed from in

Table 4. Statistics of the Surface Velocities Derived From Altimetry During the 3 Year Period, for M1, M3, and M4 and During the Periods When In Situ Velocities at 500 m Depth Were Available for M2 and M5[a]

Mooring	Altimetric Data	Weeks	Passes	Mean (cm s^{-1})	Direction of the Mean (deg)	Standard Deviation Mean	Major Axis (cm s^{-1})	Minor Axis (cm s^{-1})
M1	Gridded maps	167	-	21.4	54.3	11.4	12.8	6.1
	Jason Along Track	-	112	22.5	54.8	15.8	21.5	11.7
M2	Gridded maps	50	-	37.8	41.7	13.6	18.8	12.4
	Jason Along Track	-	-	-	-	-	-	-
M3	Gridded maps	167	-	19.7	24.5	16.2	19.4	16.7
	Jason Along Track	-	111	16.7	29.2	19.9	22.2	25.5
M4	Gridded maps	167	-	11.0	−7.7	15.7	21.9	18.6
	Jason Along Track	-	111	10.1	4.1	20.3	27.2	23.8
M5	Gridded maps	100	-	27.3	63.2	16.7	21.7	17.8
	Jason Along Track	-	69	26.3	65.9	19.4	29.8	19.9

[a]Surface velocities were derived from maps of absolute dynamic topography (gridded maps, 7 d resolution) and from Jason 1 track data (10 d resolution). M2 was not at an intersection of two Jason 1 tracks; therefore, no data from Jason tracks were available. Major axis and minor axis are the length of the standard deviation ellipse axes. Directions of the mean are in degrees (°) relative to the geographical north, and velocities are in cm s^{-1}.

situ velocities at 500 m depth for the two northernmost moorings (M1 and M2), equal for M3 and M4, and higher for M5 (Figure 7 and Tables 3 and 4). To address the lower variance of MSGV observed at M1 and M2, standard deviation ellipses of MSGV were computed using the new daily altimetric product, and standard deviation ellipses of the in situ velocities were computed using degraded data sampled every 7 d. In either case, the differences in variance at M1 and M2 were reduced by only 1 or 2 cm s^{-1}.

[41] Globally, the surface velocities derived from maps of absolute dynamic topography every 7 d and derived from Jason 1 track data every 10 d represented well the amplitude and the mean direction of the flow (except at M4). The variance was underestimated by the MSGV at the two northernmost moorings on the continental slope, and was consistent with the in situ data at M3, M4 and M5, in the center of the Yaghan Basin. The variance of the JSGV was higher than that of the in situ data, even over the continental slope. We pursued the comparisons examining time series of across-track velocities.

4.2. Time Series of Across-Track Velocity at the Mooring Locations

[42] Velocity components of the in situ velocities (1 d resolution) and of the MSGV (7 d resolution) were rotated by 43° to compute the across-track component, perpendicular to the Jason 1 track 104 (Figure 8). At M5, the extrapolated velocities at 500 m depth were considered (see section 3.3) during the period when data were missing. Correlations were then computed between the across-track components of the in situ velocities at 500 m depth and of the two sets of surface velocities derived from altimetry. Correlations between in situ velocities and JSGV were high, ranging from 0.73 (M1) to 0.87 (M4), significant at the 95% confidence level calculated according to the standard method [Emery and Thomson, 2001] (Figure 8). At M5, the correlation was 0.76, when the interpolated data were considered, and 0.86, when the period January 2007–April 2008 was not taken into account. Values were higher by 0.01 (M4) to 0.07 (M1, M5) for the correlations between the across-track components of the in situ velocities and of the MSGV (Figure 8). Despite the smaller variance at M1 and M2 of the MSGV, correlations at M1 and M2 were high (0.79 at M1 and 0.92 at M2). The comparison was also performed using the MADT with a 1 d resolution, and gave similar results.

[43] Consequently, correlations between the in situ across-track velocities at 500 m depth and the across-track component of the surface velocities derived from altimetry data were higher for the MSGV than for the JSGV at all moorings. Despite an underestimated variance at the two northernmost moorings, the MSGV, with a higher temporal resolution than the JSGV (7 d versus 10 d), were used in the following.

[44] In conclusion, the gridded maps of absolute dynamic topography, available every 7 d, performed globally well for the Yaghan Basin, but raised two main issues: a lower variation in the flow at the two northernmost moorings than that of the in situ velocities; and poor mean values near M4. Having assessed the quality of the velocity estimate based on altimetric data at the mooring location, we used the MSGV to examine the two-dimensional surface flow field to gain further insight into the in situ measurements at the moorings.

5. Interpretation of the Current Meter Data in the Light of Altimetry

[45] We first examined across-track velocities along Jason track 104 over the mooring period, to provide a spatial background for the separate in situ measurements, and over the 18 yearlong altimetric time series to put the results for the mooring period into perspective. Second, we studied the principal modes of variation in the mooring array data and in the altimetric data in the Yaghan Basin. Finally, we inspected several remarkable situations noticed in the current meter data in section 3.1.

5.1. Across-Track Velocities Along Track 104 Between 55.3°S and 58°S

[46] The high values in the across-track velocities (for the MSGV) to the north of 56°S, with a local maximum of 34.7 cm s^{-1} in the 3 year mean velocities near the M2 location, were associated with the position of the SAF (Figures 9a and 9b). The position of the Polar Front corresponded to the large across-track velocities south of 57°S. Highly variable SAF positions, reaching as far south as 57°S, were observed from April to October 2006, while large oscillations in the PF position were seen in March 2008 (Figure 9a). Such particular events (marked with a dashed blue line in Figure 9a) are examined in section 5.3. Some of them correspond to the remarkable situations noticed in the current meter data in section 3.1.
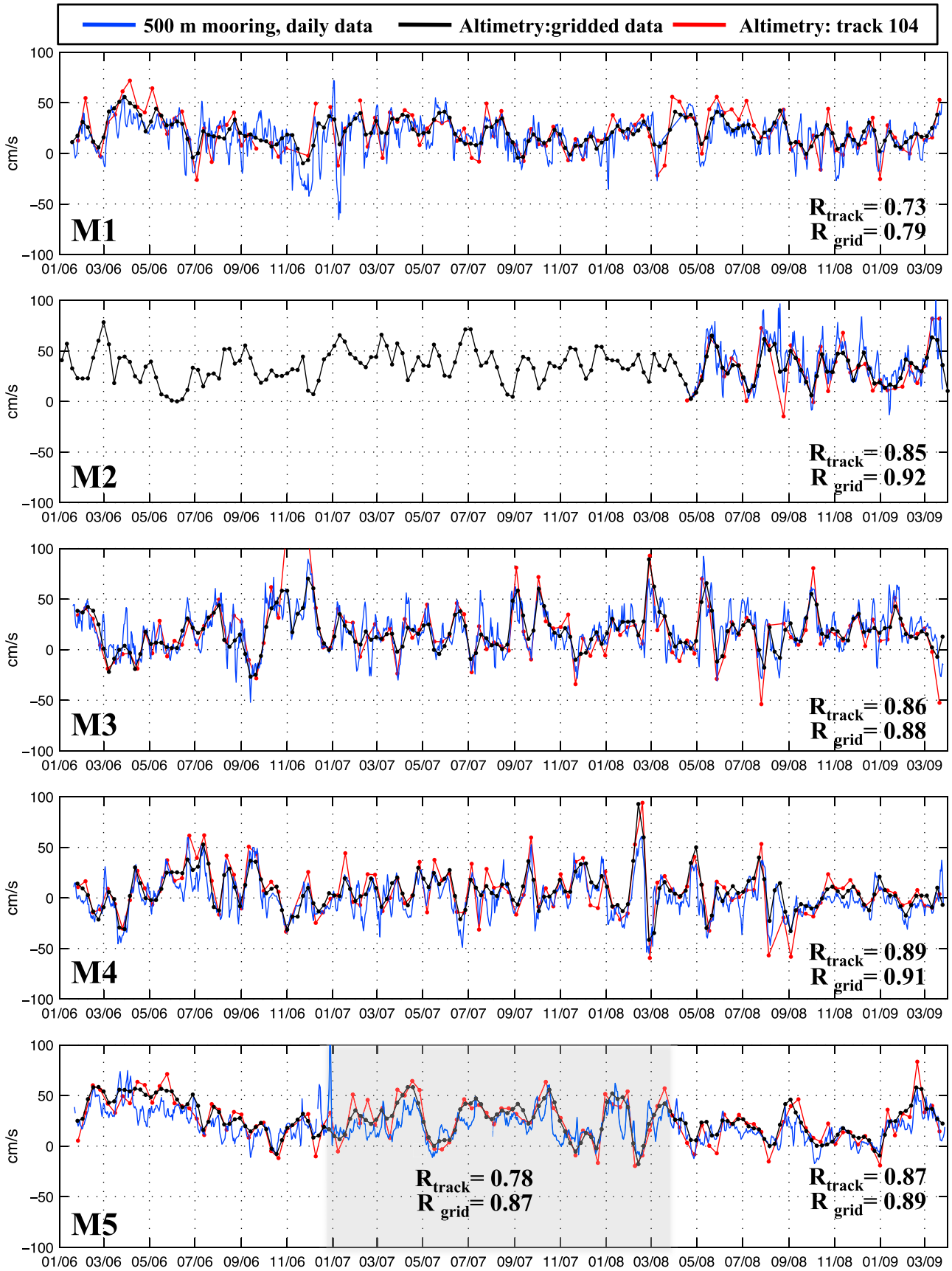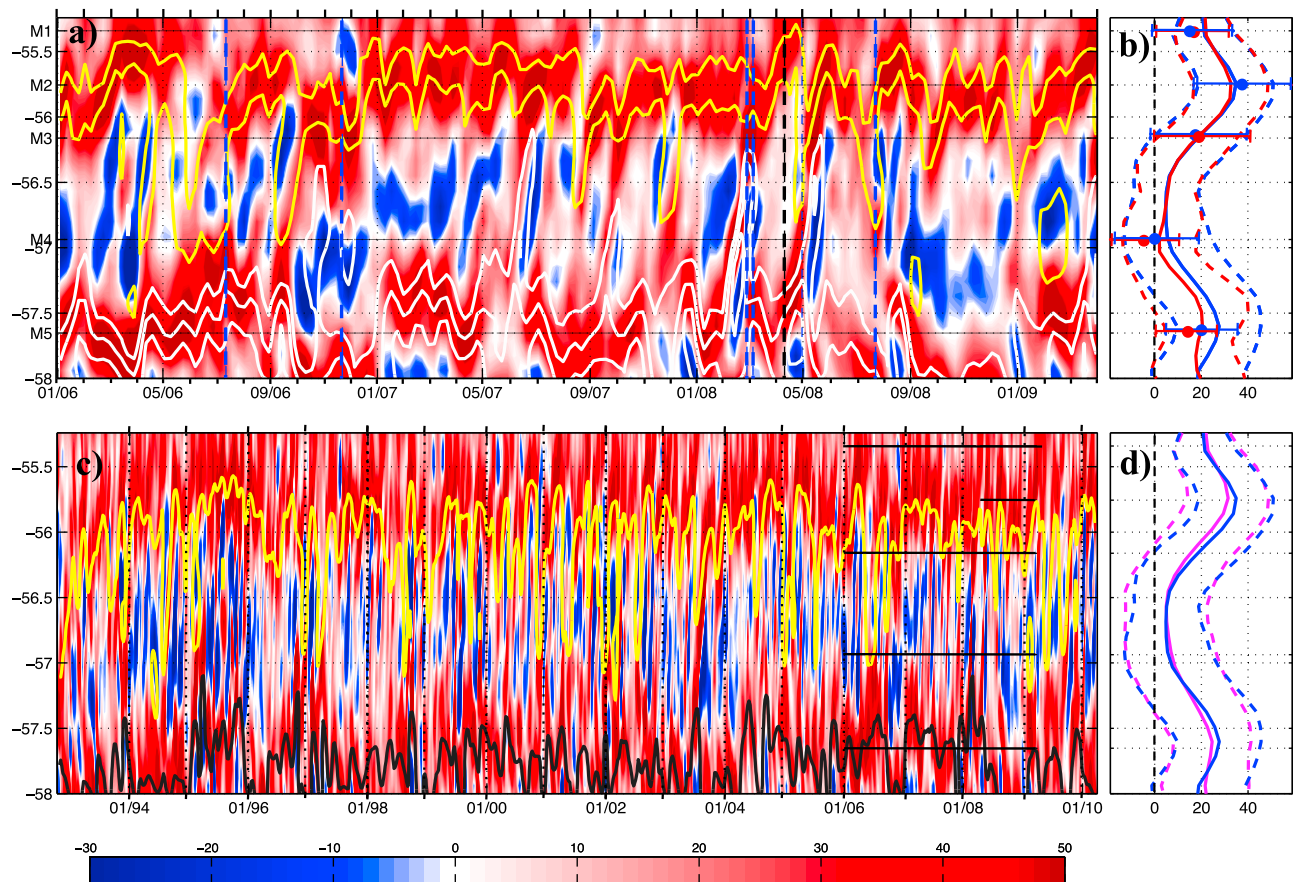
Figure 8

Figure 9. Time series of across-track velocities perpendicular to Jason track104 between 55.3°S and 58°S. (a) Time series of across-track surface geostrophic velocities derived from MADT between 18 January 2006 and 24 March 2009 and (c) for the period 1992–2011. Black horizontal lines indicate the mooring positions and their sampling duration. Vertical dashed blue and dashed black lines indicate the exceptional events studied in section 5.3. Color bar below indicates velocity in cm s^{-1}. In Figure 9a location of Subantarctic Front (SAF) branches are shown in yellow and location of Polar Front (PF) branches in white. In Figure 9c, for sake of clarity, only the locations of the southern branch of the SAF (yellow) and of the middle branch of the PF (black) are shown; they were calculated using a 28 d running mean of MADT. (b) Mean and standard deviation of the across-track component. Mean across-track velocity for MADT-based surface velocities over the period 2006–2009 is plotted in blue, and for the period 2008–2009 in red (solid: mean; dashed: mean plus or minus the standard deviation). The mean and standard deviation of the across-track velocity from in situ data for the periods 2006–2009 and 2008–2009 are plotted in blue and red dots, respectively. (d) Mean across-track MADT-based velocity for the period 1992–2011 is plotted in cyan, and the mean across-track velocity for the period 2006–2009 in blue (solid: mean; dashed: mean plus or minus the standard deviation).

[47] The mean MSGV profile during the second deployment showed noticeably lower velocities south of 56.7°S (Figure 9b) than in the first deployment. Negative across-track velocities frequently observed between the two frontal regions led to a local minimum of 4.8 cm s^{-1} in the mean across-track velocities at 56.8°S during the first deployment and of 2.0 cm s^{-1} at 57°S during the second deployment (Figures 9a and 9b). The differences in the mean MSGV profiles between the first and second deployment may be attributable to the large southward meanders of the SAF from April to October 2006. These southward meanders of the SAF were associated with high eastward velocities at M4 and M5 (Figure 3), the SAF and PF becoming adjacent to each other (see section 5.3).

[48] At the M1 and M5 locations, the mean across-track MSGV exceeded the mean in situ across-track velocity by

Figure 8. Correlation between the across-track component of the surface velocities derived from altimetry (in black and red) and from the in situ velocities at 500 m depth (in blue) between January 2006 and March 2009. The surface velocities shown in black were computed from MADT, with a 7 d resolution. The surface velocities shown in red were computed from the along-track data of Jason 1 on track 104, with a 10 d resolution. The shaded area at M5 indicates the period over which the data at 500 m depth were interpolated (sections 3.3 and 4.2).

about 5 to 8 cm s^{-1} (Figure 9b). In contrast, at M2, the mean across-track MSGV (over the period 2008–2009) was smaller than the mean across-track in situ velocity by 5 cm s^{-1} (32.9 cm s^{-1} versus 37.6 cm s^{-1}). At the M3 location, the 3 year mean across-track MSGV was identical to the mean in situ cross-track velocity (18.4 and 18.7 cm s^{-1},

respectively). At M4, the mean across-track in situ velocity was negative (i.e., westward velocities), whereas the mean MSGV was positive, the difference between the two being about 6 cm s^{-1}. Taking into account the depth of the in situ velocities and the vertical shear observed in the mean velocity throughout the water column, the comparison
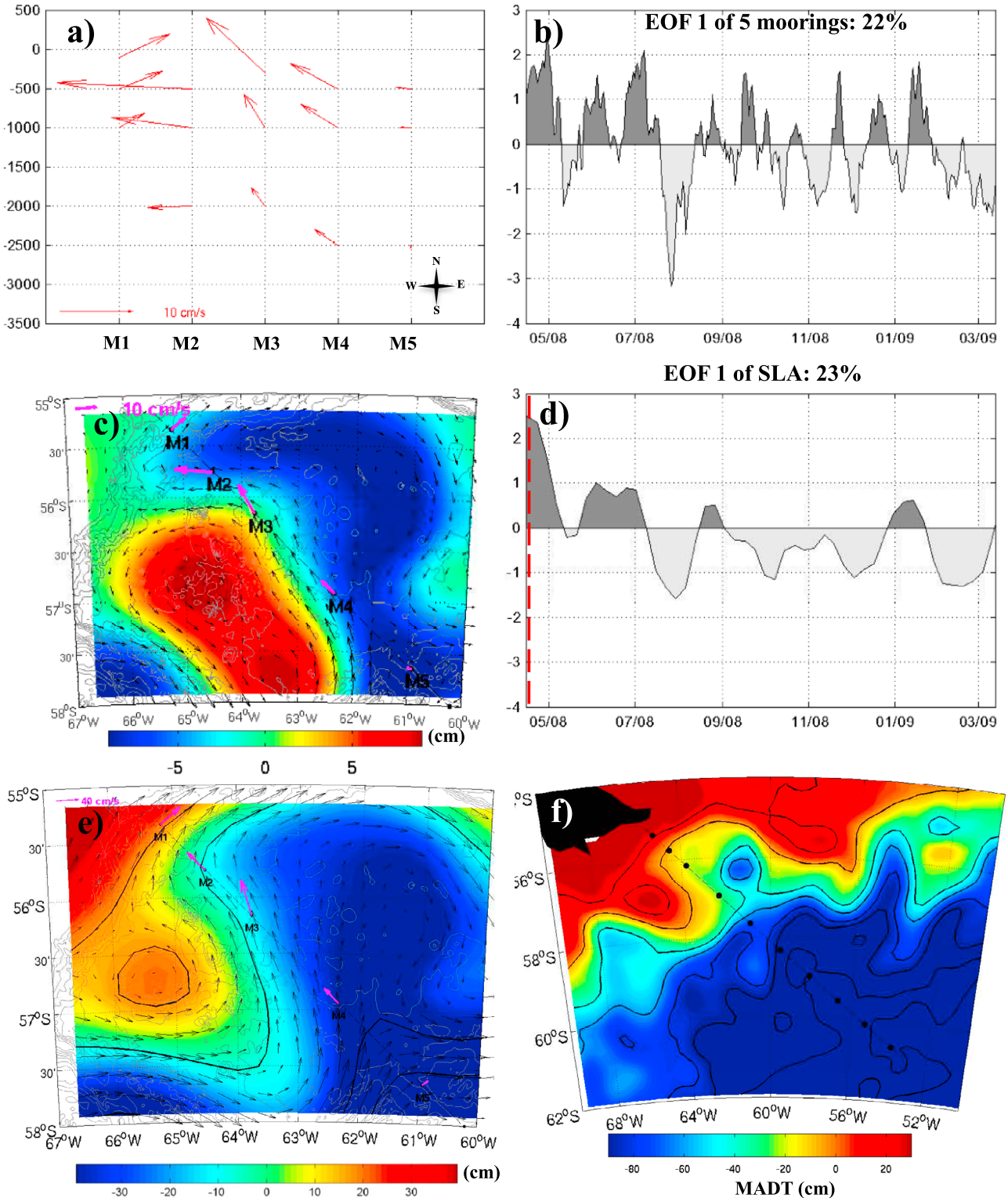

Figure 10

suggested that the mean across-track MSGV profile along track 104 was too smooth, with, for example, eastward velocities being underestimated at the M2 location by at least 10 cm s^{-1} and, likewise, westward velocities being underestimated at M4.

[49] The standard deviation of the across-track velocities reflected what was observed with the standard deviation ellipses: the across-track MSGV variance was lower than the in situ velocity variance at M1 and M2, similar to the in situ velocity variance at M3 and M4, and exceeded the in situ variance at M5 (Figure 9b).

[50] We made use of the full altimetry record (1992–2010) to appreciate the situation in the Yaghan Basin over a longer period and to put the mooring period into perspective (Figure 9c). Globally, the positions of the SAF and the PF along the track covaried, as observed by *Chouaib et al.* [2006]. However, this general covariance broke down on several and short-lasting occasions, when large meanders of the SAF reached 57°S. The beginning of the mooring period, with the 6 monthlong high velocities associated with the southward meanders of the SAF joining the PF, and the subsequent 4 monthlong strong cyclonic circulation between the SAF and the PF, was highly noticeable in the 18 yearlong time series. The year 1995 stood out in the time series, with a particularly large frequent occurrence of westward velocities.

[51] The profile of the 18 year mean across-track velocities was smoother than the mean profile over the 3 year mooring period (Figure 9d). During the mooring period, the local maxima in across-track MSGV associated with the SAF and PF were stronger by 4 cm s^{-1} and were located more toward the center of the Basin (Figure 9d). The local minimum in mean velocities during the mooring period was at the same location (56.7°S) with the same value (5 cm s^{-1}) as during the whole altimetry period. The standard deviations were similar, the only difference being observed in the center of the Basin (around 56.5°S), with the mooring period presenting a somewhat smaller mean standard deviation than the 18 year mean standard deviation.

5.2. Principal Modes of Variation in the Current Meter and Altimetry Data for the Yaghan Basin

[52] An EOF analysis was performed using the five moorings all together over the sampling time of M2 (April 2008 to March 2009), with three current meters at each mooring. The first EOF explained 22% of the total variance (Figures 10a and 10b). At each mooring, the EOF vectors at different depths were almost parallel to each other. Velocity variations at mooring M5 were weakly correlated with velocity variations at the four other moorings.

[53] To better comprehend the modes of covariation of the five mooring data sets, an EOF analysis was performed on the maps of sea level anomaly (MSLA) over the same period and over a region of the Yaghan Basin centered on the mooring array. The first EOFs explained 23% of the variance (Figures 10c and 10d). The spatial structure of the first EOF of SLA matches in strength and direction the upper vectors of the first EOF of the five mooring data sets (Figure 10c). In spite of the presence of high frequencies, the time series associated with the EOF-1 of the five moorings (Figure 10b) was remarkably similar to the time series associated with the EOF-1 of the SLA over the Yaghan Basin (Figure 10d).

[54] The spatial structure of the first EOF of MSLA corresponded to a dipole with the mooring section being located roughly between the positive and negative parts of the dipole. The maximum of the time series of the first EOF in SLA was reached on 10 April 2008 (Figure 10d). When adding the Mean Dynamic Topography, EOF-1 corresponded in its positive phase to a large southward meander of the SAF over the northern part of the SFZ upstream of the section and to a northward meander of the PF to the east of 62.5°W (Figure 10e). The MADT of 9 April 2008 (Figure 10f) showed similar spatial structure in the Yaghan Basin, with the presence of a cyclonic eddy, to the east of the M3 and M4 locations, which separated from the northward meander of the PF. In its negative phase (not shown), a PF meander was forming upstream of the section and an SAF meander downstream of the section.

[55] An EOF decomposition of SLA variations was performed with the 18 years of altimetric data. The first EOF was similar to the one obtained over the 2008–2009 period, a dipole with, in its positive phase, a southward meander of the SAF upstream of the section and negative anomalies in the northeastern part of the YB, which possibly linked to the topographic feature and explained a similar amount of the total variance (23%) (Figures 11a and 11b). This first EOF mode was a robust dominant mode. It showed up as the first mode in the several EOF decompositions we produced using either the current meter array (without M2) over the period 2006–2009 or the SLA over the period 2006–2009 and always explained more than 20% of the variance. Auto-correlations suggested a persistence of about 70 d. Wavelet transforms (not shown) showed that time scales associated with the first EOF varied from 50 to 230 d (above the 95% confidence limit) with a clear peak (above the 99% CL) at the semiannual period and some energy at the annual period. Oscillations with a 2 month time scale were observed at the beginning of the mooring deployment period, while a

Figure 10. EOF analysis of the sea level anomaly (SLA) over the Yaghan Basin (55°–58°S, 60°–67°W) and of the five moorings taken together. (a) EOF-1 of the five moorings all together (22% of the explained variance). Velocity scale in the lower left corner, compass direction in the lower right corner. (b) Time series associated with EOF-1. (c) EOF-1 (in centimeters) of SLA (23% of the explained variance). Black arrows indicate the geostrophic velocities derived from the EOF-1 of SLA. Pink arrows show the EOF-1 of the five moorings all together at 500 m depth, corresponding to Figure 10a. Velocity scale is shown in the upper left corner. (d) Time series associated with EOF-1 of SLA. The dashed red line indicates the maximum of the time series. (e) Absolute dynamic topography (ADT) corresponding to the maximum of the time series associated with EOF-1 of SLA (10 April 2008, indicated on Figure 10d by dashed red line). Black arrows indicate the geostrophic velocities derived from the MDT Pink arrows at the mooring locations correspond to the mean in situ velocity at 500 m over 7 d centered on 10 April 2008. Velocity scale is shown in the upper left corner. (f) MADT corresponding to 9 April 2008 over the Drake Passage (54°–62°S, 50°–70°W).

FERRARI ET AL.: CIRCULATION IN THE YAGHAN BASIN
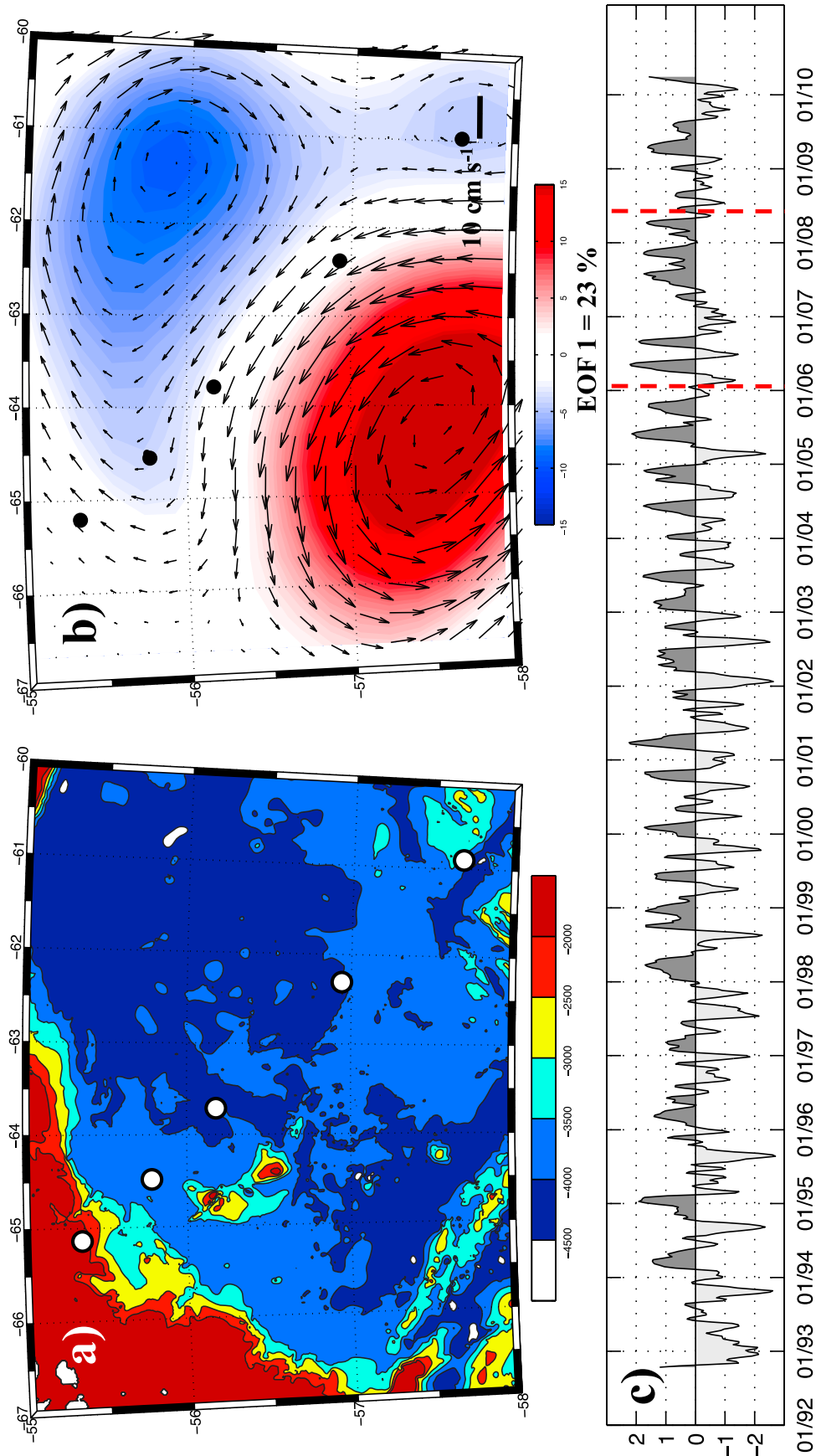
Figure 11. (a) Seafloor topography of the Yaghan Basin. (b) First EOF of the SLA over 55°–58°S, 60°–67°W during the period 1992–2011. It explains 23% of the total variance. (c) Associated time series. Red dashed lines indicate the duration of the mooring data.
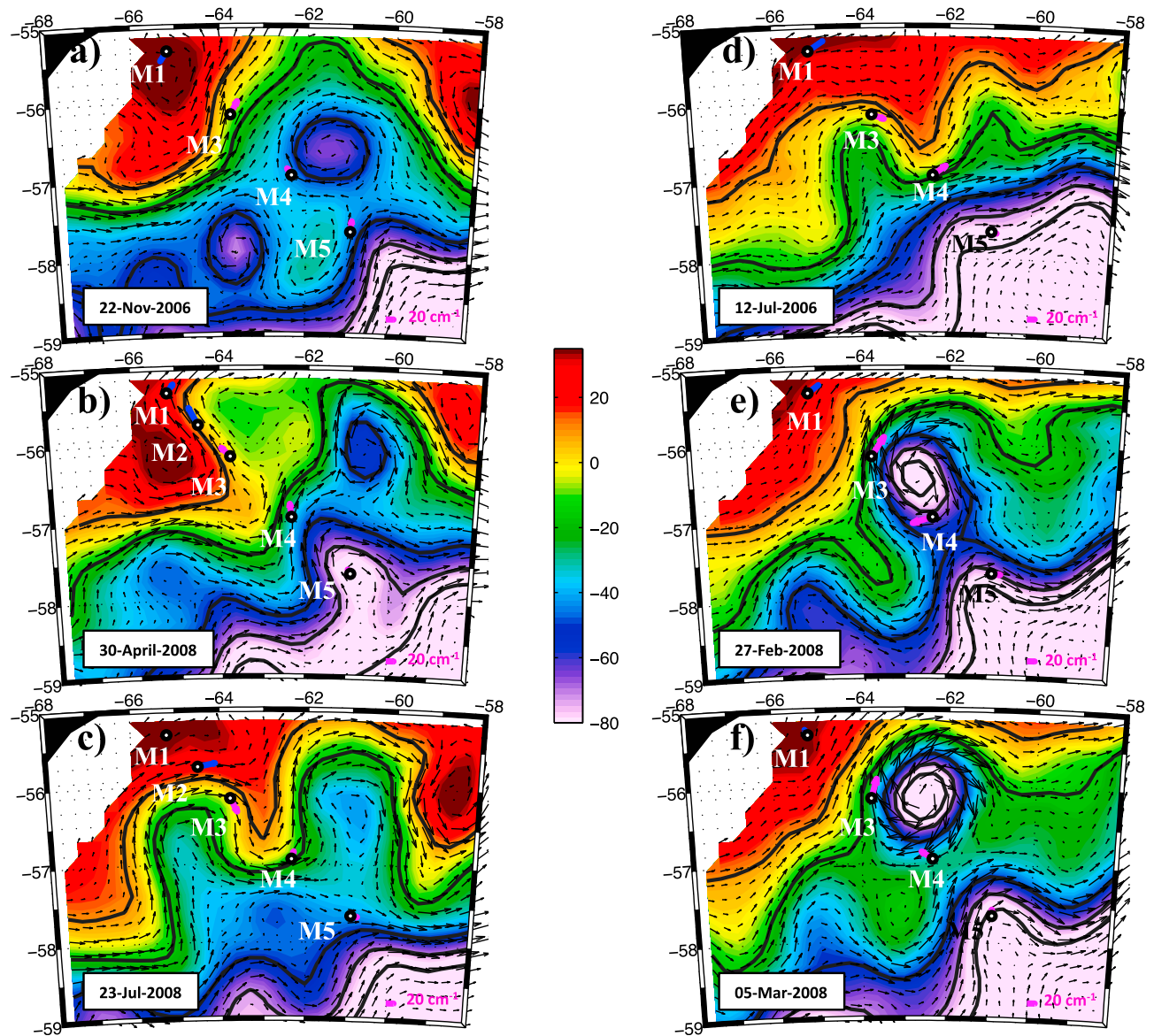
Figure 12. Maps of absolute dynamic topography of exceptional events studied in section 5.3 (in centimeters). The solid black lines are iso contours of absolute dynamic topography and correspond roughly to the mean positions of the frontal branches. For each mooring, the mean in situ velocity at 500 m depth is computed over 7 d centered on the date of each map and is shown by solid blue/rose arrows. Velocity scale in indicated in the lower right corner.

positive state lasted for a year from May 2007 to May 2008 (Figure 11c).

[56] The two subsequent modes provided by the EOF analyses of the variations in the in situ velocity of the mooring array, in the concomitant SLA field variations over the 18 years explained a comparable lower percentage of variance (12%), which is a sign of degeneration or of propagation features that are hard to compare. No physical meaning should be extracted from these modes.

5.3. Remarkable Events in the Current Meter Data in the Light of Altimetry

[57] MADT maps (Figure 12) were used to interpret remarkable situations observed in the mooring data (section 3.1). The selected dates are shown on Figure 9a.

[58] A flow with a westward component was observed over the whole water column at M1 on several occasions; for example, end of June 2006 or November 2006. The two situations were similar and MADT maps showed a small and strong anticyclonic eddy (diameter 80 km) propagating along the continental slope (Figure 12a).

[59] Large northwestward velocities (>80 cm s^{-1}) observed at M2 in April/May 2008 corresponded to the flow along the eastward side of a sharp meander of the SAF (Figure 12b). The velocities at M3 were also northwestward. The MADT velocities had the right direction and amplitude (50 cm s^{-1}). This situation is recurrent and corresponds to a large positive phase of EOF-1 (see section 5.2).

[60] At M3, large southward velocities (reaching 60 cm s^{-1}) were observed at the end of July 2008. They corresponded to
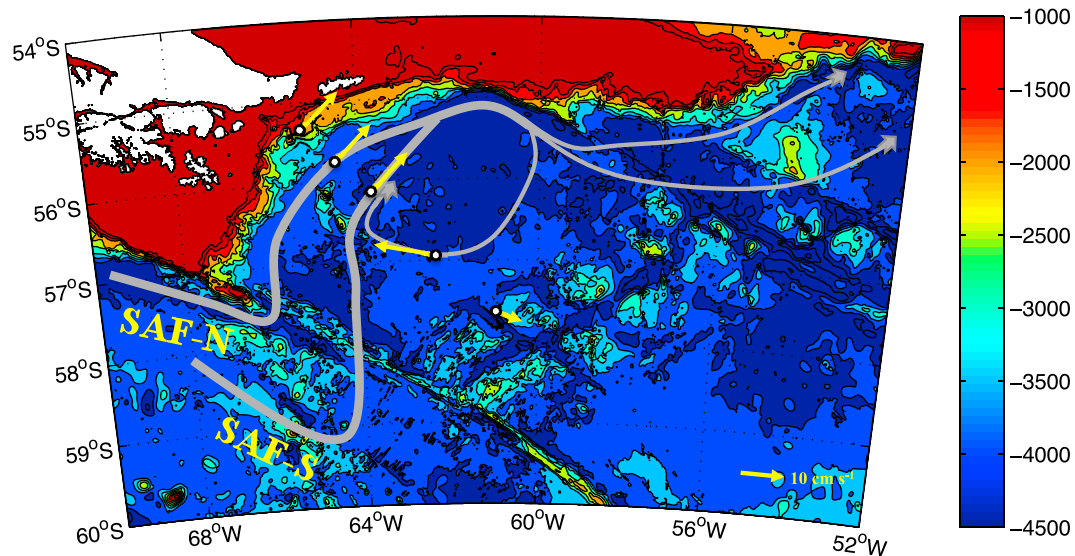
Figure 13. Schematics the permanent deep cyclonic circulation in the Yaghan Seafloor Depression. Velocities at mooring locations, indicated by yellow arrows, correspond to the mean values at the lower current meters. Velocity scale in indicated in the lower right corner. SAF-N: Subantarctic Front–Northern branch; SAF-S: Subantarctic Front–Southern branch.

the westward side of a sharp meander of the SAF propagating eastward (Figure 12c). This situation corresponds to the negative phase of EOF-1.

[61] The strong eastward velocities noticed at M4 from June to August 2006 corresponded to a particular period when the SAF and PF were close to each other, the PF being in a northern location to the north of the WSR and a southward meander of the SAF reaching as far south as M4 (Figure 12d).

[62] In February and March 2008, M3 and M4 experienced the largest vertical displacements as they were pulled down over a depth range of almost 1000 m. The amplitude and direction of the velocities at M3 and M4 suggested a strong cyclonic eddy between 25 February and 5 March 2008. On 1 March, velocities at M3 exceeded 50 cm s^{-1} at 900 m depth and 40 cm s^{-1} at 2000 m depth, with a north-northeastward direction. At the same time, velocities at M4 exceeded 60 cm s^{-1} at 500 m and 1000 m depths, and 40 cm s^{-1} at 2500 m depth, with a westward direction (Figures 3 and 12e). Simultaneous maps of dynamic topography revealed the generation of a cyclonic eddy from a meander of the PF that could be traced back in time to the end of January 2008. A northward PF meander developed until a cyclonic eddy was spawned around the location of M3 and M4 at the end of February. The cyclone corresponded to a sea level anomaly below −60 cm, and large velocities over the entire water column. At the bottom, velocities greater than 40 cm s^{-1}, peaking at 55 cm s^{-1}, were observed close to M4 during the same period by *Chereskin et al.* [2009, Figure 4].

6. Synthesis and Discussion

[63] Current meter data obtained at five mooring sites across the Yaghan Basin with two consecutive deployments totaling over 3 years' duration (from January 2006 to April 2008) have been analyzed. Altimetrically derived surface geostrophic velocities have been compared to upper-level high temporal resolution in situ velocity data for the first time in the DP. This comparison is a stringent test because of the high kinetic energy and small scales in the region. The quality and limitations of the altimetric surface geostrophic velocity estimates having been assessed, altimetry was used to interpret the observations at the isolated mooring sites and to put them in the context of the 18 yearlong altimetry time series. We recall the major results and draw the corresponding conclusions.

6.1. Current Meter Observations: Means and Vertical Velocity Structure

[64] Mooring M4, in the center of the Yaghan Basin, stood out, with a westward mean flow over the two deployments at all depths. This westward mean flow was quasi-barotropic during the second deployment and depth-intensified during the first one. This westward mean flow suggested the existence of a mean cyclonic recirculation in the Yaghan Basin. The persistent westward velocities at depth (Figure 3), with a mean westward velocity (14 cm s^{-1}) larger than the standard deviation ellipse axes, hinted at a permanent deep cyclonic circulation over the Yaghan seafloor depression (Figure 1b) with the shallow topography to the left of the current direction, as expected in the southern hemisphere. This deep cyclonic circulation is an important feature, as velocities at 2500 m depth at M4 often exceed 20 cm s^{-1} (Figure 3). The 1 year mean near-bottom velocities in *Chereskin et al.* [2009] also suggest a deep cyclonic circulation in the YSD, with means exceeding variability [*Chereskin et al.*, 2009, Figure 1]. The deep cyclonic circulation schematically represented in Figure 13 is forced by the bottom-reaching SAF flow which enters the YSD in the north and is then constrained by the topography.

[65] Mean velocities for the two deployments (26 months and 12 months, respectively) were slightly different at M4 and M5, and this may be explained by the numerous southward meanders of the SAF in the first part of the first

mooring deployment. These southward meanders of the SAF corresponded to eastward velocities at M4 (Figures 4 and 9). Apart from the noticeable exception of mooring M4 discussed above, mean velocities were surface intensified. A small counterclockwise rotation of the mean velocity vectors with depth at M3 below 500 m (Figure 4) was consistent with a mean downwelling induced by the deepening of the seabed (YSD) past a topographic obstacle upstream (YS; Figure 1b).

[66] An EOF analysis of the vertical structure of velocity variations at each mooring showed that the first two modes explaining most of the variance were parallel to the standard deviation ellipse axes and were surface intensified, confirming a barotropic-equivalent structure of the flow variations. This is consistent with the analysis of the DRAKE 79 data by *Inoue* [1985]. At M3, M4 and M5, an energetic 15–60 d period, a typical time scale of mesoscale activity, is observed in the time series associated with the first and second EOF.

[67] On the continental slope at M1, the first EOF, in the direction of the mean flow, dominated, explaining 74% of the variance and showing a clear annual cycle, with maximum velocities in austral summer and minimum, in austral winter (Figure 6). The second EOF, with higher frequencies (5 to 15 d), reflected the signature of baroclinic coastal-trapped waves (CTW). These are also observed to a lesser extent at M2. The existence of CTW with periods of a few days to weeks has been demonstrated along various coastlines around the world: off the coast of South Africa [*Schumann and Brink*, 1990], off the coast of Australia [*Freeland et al.*, 1986]. Coastal-trapped waves were observed on the western coast of South America [*Clarke and Ahmed*, 1999], with a poleward propagation of 250 km d^{-1}, and by *Vivier et al.* [2001] in the Malvinas Current. In 2006, during the two crossings of the Drake Passage along Jason 1 track 104, *Renault et al.* [2011] observed deep westward velocities (at 1000–4000 m depth) below an eastward flow (0–1000 m depth) along the American continental slope, indicating the presence of baroclinic coastal-trapped waves. The CTW activity was nonstationary, with a greater energy during the first deployment than during the second (standard deviation ellipses at depth were larger at M1 during the first deployment than during the second).

6.2. Satellite-Derived Surface Geostrophic Velocities

[68] Globally, altimetrically derived velocities compared rather well with the in situ velocities at 500 m depth over the 3 year period (2006–2009), in strength and direction. At M4, the direction of the altimetrically derived mean velocities, although different from that of the mean in situ velocity at 500 m depth, was consistent with the counterclockwise veering with depth observed in the mean in situ velocities. The mean altimetrically derived velocities were larger than the in situ velocities by 5 to 8 cm s^{-1} at M1 and M5, as expected, and underestimated by 4.7 cm s^{-1} at M2 (which is near the mean position of the SAF).

[69] Correlations were high (between 0.73 and 0.92) between the across-track velocities, in situ velocities at 500 m depth, MSGV and JSGV over the 3 year period (2006–2009). The variance at M1 and M2 was underestimated by the MSGV, was equal to the in situ values at M3 and M4 and was larger at M5. The velocity variance

of the JSGV was larger for all moorings than the variance of the in situ velocities at 500 m depth.

[70] Altimetry helped in the interpretation of the remarkable situations observed in the mooring data. One of these is the cyclonic eddy observed in March 2008 (section 5.3), the strongest observed in the Yaghan Basin between January 2006 and March 2009. It was detected by altimetry, by current meters throughout the water column (in this paper) and by near-bottom current meters [*Chereskin et al.*, 2009]. Altimetry documented its development from a northward meander of the PF, advancing first eastward and then northward. Cyclonic eddies are frequently observed in the Yaghan Basin [*Barré et al.*, 2011] and act as a mechanism for ventilation of the Antarctic Intermediate Water to the north of the Polar Front by Winter Water (WW) (between 100 and 500 m depths) [*Provost et al.*, 2011].

[71] Modes of velocity variation in the Yaghan Basin were examined using altimetry (over different time periods) and the five-mooring array. A dominant mode explaining 23% of the variance corresponded, in its positive phase, to a strong southward meander of the SAF upstream of the section and a northward meander of the PF or a cyclonic eddy to the east of the section. The upper vectors (at 500 m depth) of the first EOF of the five-mooring array (22% of the variance) were in good agreement with the spatial pattern of the first EOF of SLA (23% of the explained variance), and the respective associated time series also bore similarities. The 18 yearlong altimetry time series revealed that this mode was robust, dominant and had a strong semiannual component. This mode corresponded to the eastern part of the recurrent dipole structure at the entrance to DP over the northern parts of the PAR and the SFZ [*Barré et al.*, 2011, Figures 13 and 16]. The subsequent two modes were degenerate. It was noted that velocity variations at M5 were weakly correlated with velocity variations at the other moorings in the Yaghan Basin. Indeed, velocity variations are associated with the PF meanders over the West Scotia Ridge, as shown by *Ferrari et al.* [2012].

Appendix A

[72] The strong velocities encountered in the Drake Passage caused the moorings to make vertical excursions, typically less than 100 m. However, moorings M3 and M4 had excursions exceeding 500 m more than a dozen times in three years. Therefore, as a first step before interpreting temperature and velocity data, the mooring measurements were interpolated (and extrapolated) to fixed depths using a mooring motion-correction scheme adapted from *Hogg* [1991], *Cronin and Watts* [1996] and *Phillips and Rintoul* [2000]. Nominal pressures were chosen close to the minimum pressure of each instrument. This scheme, which compensates both the temperature and velocity measurements for mooring motion, assumes that the depth range between any two isotherms is constant so that a canonical temperature profile can be defined:

$$T(p) = F(p - p_{ref}).$$

[73] The canonical profile (F) is a third-order polynomial determined by a least squares fit applied to each mooring data. Each mooring canonical profile was compared with the
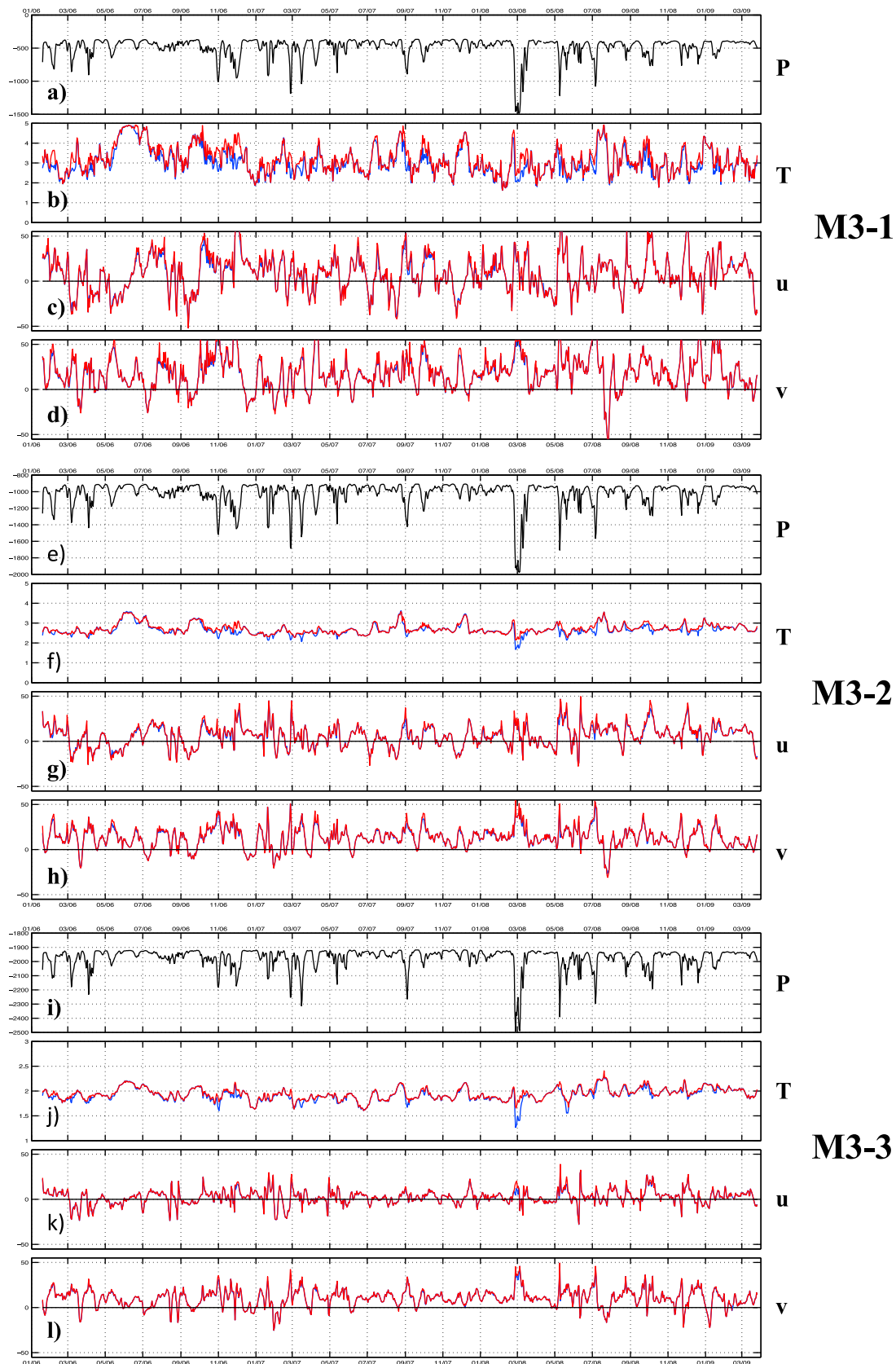
Figure A1. Example of mooring correction for M3 at three levels (M3-1, M3-3, M3-4): (a, e, and i) Pressure time series (in dbars), (b, f, and j) temperature time series (in °C), (c, g, and k) zonal component (*u*) time series, and (d, h, and l) meridional component (*v*) time series (in centimeters per second). For temperature, *u* component, and *v* component, corrected values are plotted in red and original values in blue.

conductivity-temperature (CTD) data obtained during 2006, 2008 and 2009 oceanographic surveys at the mooring location, and was used to calculate the compensated temperature, T_c, at the nominal pressure, p_{nom}: $T_c = F(p_{nom} - p_{ref})$. The temperature correction scheme was modified by *Cronin and Watts* [1996] to ensure that the corrected temperature, T_c, smoothly approaches the measured temperature, T_{meas}, when the current meter pressure, p_{meas}, approaches the nominal pressure, p_{nom}: when $p_{meas} = p_{nom}$, $T_c = T_{meas}$.

[74] The velocity measurements were computed at p_{nom} by using the *Cronin and Watts* [1996] scheme of interpolating and extrapolating on temperature:

$$u_c = \frac{u_u - u_l}{T_u - T_l}(T_c - T_l) + u_l$$

$$v_c = \frac{v_u - v_l}{T_u - T_l}(T_c - T_l) + v_l$$

[75] Where u and v are the west–east and north–south velocity components; the subscript c refers to the corrected measurement at p_{nom}, and the subscripts u and l refer to the upper and lower instrument measurement on the same mooring.

[76] The correction for mooring motion was applied to all instruments. Maximal vertical excursions varied between 73 m (M1-3) to 1584 m (M4-1) (Table 1). As an example, the correction of the temperature and velocity measurements is shown (Figure A1) for mooring M3, which was pulled down 1119 m, maximum, during the first period and 828 m, maximum, during the second period (Table 1). Maximal corrections were made for the upper instruments and reached $1°C$ in temperature and 8 cm s^{-1} in velocity (M3-1 in March 2008). Significant corrections are observed when a mooring makes large excursions. The difference in temperature is always positive; when the mooring is pulled down, the measured temperature is lower than the temperature at the nominal depth. Similarly, the absolute velocity at the nominal depth (u and v components) is increased compared to the measured velocity. The impact of the correction for mooring motions on the velocity statistics is small, whereas the corrections for temperature are important, since they will be used in heat-flux calculations, which require an accurate temperature.

References

Barré, N., C. Provost, A. Renault, and N. Sennéchal (2011), Mesoscale activity in Drake Passage during the cruise survey ANT-XXIII/3: A satellite perspective, *Deep Sea Res., Part II*, 58, 2533–2554, doi:10.1016/j.dsr2.2011.01.003.

Brink, K. H. (1991), Coastal-trapped waves and wind-driven currents over the continental shelf, *Annu. Rev. Fluid Mech.*, 23, 389–412, doi:10.1146/annurev.fl.23.010191.002133.

Chereskin, T. K., K. A. Donohue, D. R. Watts, K. L. Tracey, Y. L. Firing, and A. L. Cutting (2009), Strong bottom currents and cyclogenesis in Drake Passage, *Geophys. Res. Lett.*, 36, L23602, doi:10.1029/2009GL040940.

Chouaib, N., F. Stoehr, and C. Provost (2006), Variability of the Subantarctic and Polar fronts in the Drake Passage as deduced from altimetry, *J. Mar. Res.*, 64, 669–693, doi:10.1357/002224006779367276.

Clarke, A. J., and R. Ahmed (1999), Dynamics of remotely forced intraseasonal oscillations off the western coast of South America, *J. Phys. Oceanogr.*, 29(2), 240–258, doi:10.1175/1520-0485(1999)029<0240:DORFIO>2.0.CO;2.

Cronin, M., and D. R. Watts (1996), Eddy-mean flow interaction in the Gulf Stream at 68°W. Part I: Eddy energetics, *J. Phys. Oceanogr.*, 26, 2107–2131, doi:10.1175/1520-0485(1996)026<2107:EFIITG>2.0.CO;2.

Cunningham, S. A., S. G. Alderson, B. A. King, and M. A. Brandon (2003), Transport and variability of the Antarctic Circumpolar Current in Drake Passage, *J. Geophys. Res.*, 108(C5), 8084, doi:10.1029/2001JC001147.

Ducet, N., P.-Y. Le Traon, and G. Reverdin (2000), Global high-resolution mapping of ocean circulation from TOPEX/Poseidon and ERS-1 and -2, *J. Geophys. Res.*, 105, 19,477–19,498, doi:10.1029/2000JC900063.

Emery, W. J., and R. E. Thomson (2001), *Data Analysis Methods in Physical Oceanography*, 2nd ed., Elsevier, Amsterdam, Netherlands.

Ferrari, R., C. Provost, N. Barré, N. Sennéchal, and J.-H. Lee (2012), Circulation in the Drake Passage revisited using new current time series and satellite altimetry: 2. The Ona Basin, *J. Geophys. Res.*, doi:10.1029/2012JC008193, in press.

Firing, Y. L., T. K. Chereskin, and M. R. Mazloff (2011), Vertical structure and transport of the Antarctic Circumpolar Current in Drake Passage from direct velocity observations, *J. Geophys. Res.*, 116, C08015, doi:10.1029/2011JC006999.

Freeland, H. J., F. M. Boland, J. A. Church, A. J. Clarke, A. M. G. Forbes, A. Huyer, R. L. Smith, R. O. R. Y. Thompson, and N. J. White (1986), The Australian Coastal Experiment: A search for coastal-trapped waves, *J. Phys. Oceanogr.*, 16, 1230–1249, doi:10.1175/1520-0485(1986)016<1230:TACEAS>2.0.CO;2.

Hofmann, E. E., and T. Whitworth (1985), A synoptic description of the flow at Drake Passage from year-long measurements, *J. Geophys. Res.*, 90, 7177–7187, doi:10.1029/JC090iC04p07177.

Hogg, N. G. (1991), Mooring motion corrections revisited, *J. Atmos. Oceanic Technol.*, 8, 289–295, doi:10.1175/1520-0426(1991)008<0289:MMCR>2.0.CO;2.

Hughes, C. W., P. L. Woodworth, M. P. Meredith, V. Stepanov, T. Whitworth, and A. R. Pyne (2003), Coherence of Antarctic sea levels, Southern Hemisphere Annular Mode, and flow through Drake Passage, *Geophys. Res. Lett.*, 30(9), 1464, doi:10.1029/2003GL017240.

Inoue, M. (1985), Modal decomposition of low-frequency currents and baroclinic instability at Drake Passage, *J. Phys. Oceanogr.*, 15, 1157–1181, doi:10.1175/1520-0485(1985)015<1157:MDOTLF>2.0.CO;2.

Kartavtseff, A. (2008), Mouillages Drake, courantometres–profileurs–capteurs P,T,C, POLARSTERN, Janvier 2006–Avril 2008, Rapport Interne LOCEAN, Univ. Pierre et Marie Curie, Paris.

Klinck, J. M. (1985), EOF analysis of central Drake Passage currents from DRAKE 79, *J. Phys. Oceanogr.*, 15, 288–298, doi:10.1175/1520-0485(1985)015<0288:EAOCDP>2.0.CO;2.

Meredith, M. P., et al. (2011), Sustained monitoring of the Southern Ocean at Drake Passage: Past achievements and future priorities, *Rev. Geophys.*, 49, RG4005, doi:10.1029/2010RG000348.

Nowlin, W. D., Jr., T. Whitworth, and R. D. Pillsbury (1977), Structure and transport of the Antarctic Circumpolar Current at Drake Passage from short-term measurements, *J. Phys. Oceanogr.*, 7, 788–802, doi:10.1175/1520-0485(1977)007<0788:SATOTA>2.0.CO;2.

Orsi, A., T. Whitworth, and W. Nowlin (1995), On the meridional extent and fronts of the Antarctic Circumpolar Current, *Deep Sea Res., Part I*, 42, 641–673, doi:10.1016/0967-0637(95)00021-W.

Phillips, H. E., and S. R. Rintoul (2000), Eddy variability and energetics from direct current measurements in the Antarctic Circumpolar Current south of Australia, *J. Phys. Oceanogr.*, 30(12), 3050–3076, doi:10.1175/1520-0485(2000)030<3050:EVAEFD>2.0.CO;2.

Provost, C., A. Renault, N. Barré, N. Sennéchal, V. Garçon, J. Sudre, and O. Huhn (2011), Two repeat crossings of Drake Passage in austral summer 2006: Short-term variations and evidence for considerable ventilation of intermediate and deep waters, *Deep Sea Res., Part II*, 58, 2555–2572, doi:10.1016/j.dsr2.2011.06.009.

Renault, A., C. Provost, N. Sennéchal, N. Barre, and A. Kartavtseff (2011), Two full-depth velocity sections in the Drake Passage in 2006—Transport estimates, *Deep Sea Res., Part II*, 58, 2572–2591, doi:10.1016/j.dsr2.2011.01.004.

Schumann, E. H., and K. H. Brink (1990), Coastal-trapped waves off the coast of South Africa: Generation, propagation and current structures, *J. Phys. Oceanogr.*, 20, 1206–1218, doi:10.1175/1520-0485(1990)020<1206:CTWOTC>2.0.CO;2.

Sokolov, S., and S. R. Rintoul (2009), Circumpolar structure and distribution of the Antarctic Circumpolar Current fronts: 1. Mean circumpolar paths, *J. Geophys. Res.*, *114*, C11018, doi:10.1029/2008JC005108.

Spadone, A., and C. Provost (2009), Variations in the Malvinas Current volume transport since October 1992, *J. Geophys. Res.*, *114*, C02002, doi:10.1029/2008JC004882.

Sprintall, J. (2003), Seasonal to interannual upper-ocean variability in the Drake Passage, *J. Mar. Res.*, *61*, 27–57, doi:10.1357/002224003321586408.

Vivier, F., C. Provost, and M. P. Meredith (2001), Remote and local forcing in the Brazil–Malvinas region, *J. Phys. Oceanogr.*, *31*, 892–913, doi:10.1175/1520-0485(2001)031<0892:RALFIT>2.0.CO;2.

Whitworth, T., III (1983), Monitoring the transport of the Antarctic Circumpolar Current at Drake Passage, *J. Phys. Oceanogr.*, *13*, 2045–2057, doi:10.1175/1520-0485(1983)013<2045:MTTOTA>2.0.CO;2.